Attachment 2 to PLA-6242
Appendix 2

Onset of High Frequency Flow Induced Vibration in the Main Steam Lines At Susquehanna Steam Electric Station: A Subscale Investigation of Standpipe Behavior

Revision 1

C.D.I. Report No. 05-32

Onset of High Frequency Flow Induced Vibration in the Main Steam Lines at Susquehanna Steam Electric Station: A Subscale Investigation of Standpipe Behavior

Revision 1

Prepared by

Continuum Dynamics, Inc.
34 Lexington Avenue
Ewing, NJ 08618

Prepared under Purchase Order No. 303035-C for

PPL Susquehanna, LLC
2 N 9th Street
Allentown, PA 18101-1179

Approved by

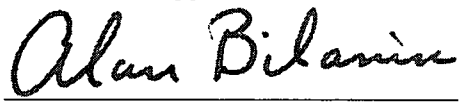

Alan J. Bilanin

Reviewed by

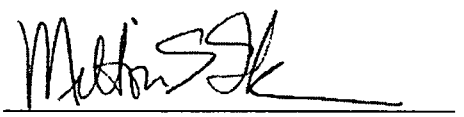

Milton E. Teske

July 2007

Executive Summary

As part of the engineering effort in support of power uprate at Susquehanna Steam Electric Station, Continuum Dynamics, Inc. undertook a subscale examination of the standpipe/valve geometry on two of the four main steam lines, in an effort to validate the frequency onset at which flow induced vibration, resulting from standpipe/valve resonance, could potentially impact steam dryer loads. In this study Continuum Dynamics, Inc. constructed a nominal one-sixth scale model of two of the main steam lines at Susquehanna Steam Electric Station, then tested the as-built configuration of standpipes and Crosby valves as appropriate. The findings suggest that no new discrete frequency sources of acoustic excitation from the main steam lines are to be expected when increasing power from CLTP to EPU conditions.

This effort provides PPL with a subscale test that suggests that new flow induced vibration loads should not play a role in the pressure loads to be experienced by the Susquehanna steam dryer at EPU conditions.

Table of Contents

I. Introduction

As part of its effort in support of power uprate at Susquehanna Steam Electric Station (SSES), PPL Susquehanna LLC contracted with Continuum Dynamics, Inc. (C.D.I.) to evaluate existing main steam line data (collected on venturi instrument lines) to estimate the pressure loads expected on the steam dryer at Current Licensed Thermal Power (CLTP). These results [1] suggest that the steam dryer stresses are acceptable at CLTP conditions. To go to higher EPU power levels, PPL requested that C.D.I. evaluate the potential for flow induced vibration (FIV) in the main steam lines as a result of resonance of the as-built standpipe/valve combination. Studies conducted by Exelon for Quad Cities Unit 1 and Unit 2 suggested that the excitation of the standpipe/valve should be explored, as this mechanism was most responsible for the pressure loading experienced on the Quad Cities steam dryers [2].

The high frequencies associated with FIV are known to correspond to a resonance associated with the inlet standpipes connected to safety valves, and have been the source of problems in several power plants in recent years [3–6]. Specifically, in [6], C.D.I. conducted a series of tests in support of damage that was observed on Columbia's main steam line safety valves. These tests concluded that the geometry of the Columbia standpipes and safety valve inlets, with flow conditions of approximately 60% to 70% of licensed power, resulted in a resonance at approximately 1050 Hz in a scaled facility (corresponding to approximately 204 Hz in the plant). The observation was made that properly scaled tests could provide data that could be used for design.

At the request of PPL, C.D.I. applied the insights gained from the study on Columbia to the SSES standpipe/valve configuration modeled protypically, as both Susquehanna units are essentially identical for the purpose of this analysis. This report summarizes the test results on two single main steam line scaled configurations.

II. Objectives

Construction of a high Reynolds number subscale test facility, simulating two of the main steam lines at SSES, was done so as to achieve the following goals:

1. Confirm that FIV of the relief valve standpipes will only occur at power levels which exceed EPU conditions.

2. Validate the analytical predictions of FIV onset power level and frequency of oscillation estimated in [7] for Crosby valves and standpipes, as built on Susquehanna main steam lines B and C.

3. Measure the FIV from Susquehanna main steam lines A and D resulting from their dead-headed branch lines as a function of power level.

III. Theoretical Approach

A subscale test facility is proposed as a means of measuring the effect of standpipes on the anticipated acoustic signal to the steam dome. A description of the phenomenon at work, analytical tools to be used, and scaling laws justifying the subscale tests are given here.

3.1 Side Branch Excitation Mechanism

The phenomenon of flow-excited acoustic resonance of closed side branches has been examined for many years (see as early as [8] and [9]). In this situation acoustic resonance of the side branch is caused by feedback from the acoustic velocity of the resonant standing wave in the side branch itself. Figure 3.1 illustrates the typical geometry used here and in the standpipes at SSES. The main steam line flow velocity U approaches an open side branch of diameter d and length L. Pressure p as a function of time t can be measured at the closed end of the pipe. The flow velocity induces perturbations in the shear layer at the upstream separation location in the main steam line. As these perturbations are amplified and convected downstream, they interact with the acoustic field and produce acoustic energy which reinforces the resonance of the acoustic mode. Ziada has studied this effect extensively [10–12], and has shown that the flow velocity of first onset of instability U_{on} corresponds to a typical Strouhal number of St = 0.55, where St is defined as

$$St = \frac{f(d+r)}{U_{on}} \tag{3.1}$$

where d is the diameter of the standpipe, r is the radius of the inlet chamfer, and f is the first mode of acoustic oscillation in the pipe system. A design chart that more accurately infers St, based on d and the diameter D of the main steam line, may be found in [10].

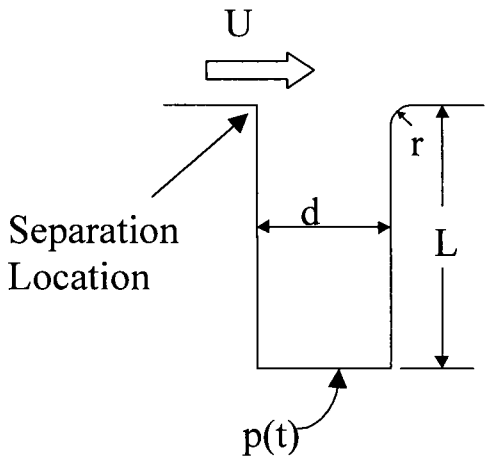

Figure 3.1. Schematic of the side branch geometry.

Solving for U_{on} in Equation (3.1), it may be seen that the onset velocity is linearly proportional to the standpipe diameter, so long as that diameter does not change the first acoustic mode frequency of the standpipe.

The implications of this side branch excitation frequency may be seen by examining the behavior of the pressure response as a function of Strouhal number (Figure 3.2). For large Strouhal numbers (beginning on the right side of the figure), the RMS pressure p_{RMS} begins increasing (at a specific onset Strouhal number and flow velocity U_{on}, depending on acoustic speed a, pipe diameter d, and pipe length L), reaches a peak value, then decreases. Flow velocity increases from right to left in this figure, where it may then be seen that this phenomenon – if it occurs in a standpipe/valve configuration – will occur at a low power level, reach a peak effect, then diminish and possibly disappear at sufficiently high power levels.

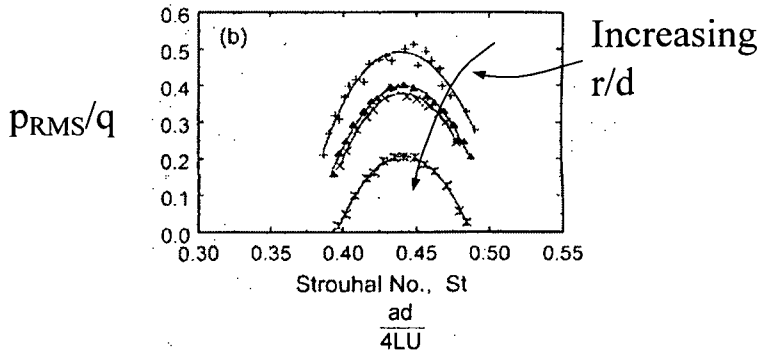

Figure 3.2. Strouhal number behavior, where q is the dynamic pressure ($\frac{1}{2}\rho U^2$), ρ is the fluid density, and a is the acoustic speed.

Initially, it may be anticipated that the first mode frequency f_1 can be approximated by the quarter-standing wave frequency of the standpipe/valve combination

$$f_1 = \frac{a}{4L} \tag{3.2}$$

Since the standpipe/valve combination changes area as a function of distance from the main steam line to the valve disk, a more accurate estimate of f_1 may be generated by including these area change effects. The combination of an accurate excitation frequency f_1 and subsequent calculation of onset velocity U_{on} with the appropriate Strouhal number then characterizes the behavior of the standpipe/valve combination considered.

3.2 Scaling Laws

By non-dimensional analysis, it may be shown from the physical parameters considered in Figure 3.1 that the unsteady pressure p(t) is

$$\frac{p(t)}{\frac{1}{2}\rho U^2} = \text{fcn}\left[M = \frac{U}{a}, \text{Re} = \frac{\rho U d}{\mu}, \frac{d}{D}, \frac{d}{L}, \frac{tU}{D}\right] \tag{3.3}$$

where ρ is the density of the fluid, μ is the absolute viscosity of the fluid, M is the Mach number, and t is time. This scaling law, developed previously by C.D.I. under EPRI sponsorship [13], shows that if acoustic phenomena are to be preserved at subscale, it is critical to preserve the Mach number M between full-scale and subscale tests. Since the nuclear power plant uses steam as a working fluid and the tests to be undertaken will use compressed air, the velocities U_s in the subscale facility will be related to the velocities U_f in the plant by

$$U_s = U_f a_s / a_f \tag{3.4}$$

Since the acoustic speed in steam at plant operating conditions is nominally $a_f = 1600$ ft/sec and the speed of sound in air is $a_s = 1100$ ft/sec, the air speeds in the subscale rig will be less than in the plant by the ratio of 11/16.

Assuming that the scale factor of the facility is $s = L_s/L_f$, where L_s and L_f are characteristic dimensions of the subscale and full-scale plant, respectively, it was also shown in [13] that the frequencies measured in the subscale rig f_s are related to those in the plant f_f by

$$f_s = f_f a_s / (a_f s) \tag{3.5}$$

so that frequencies measured at subscale are in general higher than in the full-scale plant. For the 1.0/5.87 scale tests reported herein, the frequencies measured in the subscale facility are to be multiplied by 0.2478 to obtain full-scale frequencies.

Lastly, it was shown in the previous equation and in [13], and has been reported by others as well [11], that acoustic pressures at fixed Mach number scale with the dynamic pressure in the system, and therefore scale with the system stagnation pressure. Therefore, to maximize the signal to be measured, the subscale tests should be conducted at as high system pressures as practical. It is straightforward to show that the fluctuations in pressure at subscale p_s are related to the pressure fluctuations at full scale p_f by

$$p_s/p_f = (P_s/P_f)\,(a_s^2/a_f^2) \tag{3.6}$$

where P_s and P_f are the stagnation pressures at subscale and in the plant, respectively. This relationship establishes that if it is desired to measure full-scale pressure fluctuations at subscale, the subscale system pressure would need to be raised by a_f^2/a_s^2 or by about 110% above the plant pressure, assuming air is used in the subscale facility.

Also, if subscale tests are contemplated, care should be exercised in test design to carry out the tests at as high a Reynolds number as practical, until it can be shown that the phenomenon to be investigated is insensitive over the Reynolds number ranges of interest. The

Reynolds number is defined here as the products of the steam density, steam velocity, and main steam line pipe diameter, divided by the absolute viscosity of steam or air. Since the absolute viscosity is only temperature dependent, and if acoustic phenomenon are to be examined (the velocities are fixed by Mach number scaling as discussed above), it is the product of the gas density times the diameter of the pipe that can be used to control the Reynolds number between scales. The important observation made here is that if a test is conducted where the diameter D is reduced from full scale to subscale by the scale factor s, it is advisable to increase the density of the gas by 1/s, or at least as much as practical. By conducting tests using air to replace 1000 psia steam and reducing the test rig by the scale factor s, the Reynolds number R_s of the subscale test to that of the plant R_f is

$$\frac{Re_s}{Re_f} \approx \frac{P_s}{P_f}\frac{L_s}{L_f} \tag{3.7}$$

where it has been assumed that steam can be analyzed by assuming it behaves as a perfect gas. The above relationship suggests again that subscale tests be conducted at high pressures, the higher the better. Preserving Reynolds number at subscale in general would require subscale pressures to exceed full scale pressures. Fortunately, previous testing has indicated that exact similitude of Reynolds number is not required.

Finally, it should be noted that Ziada [10] argued that while subscale tests must be used with care when inferring amplitudes, the onset of the resonance appears to be reasonably insensitive to scale. It is suspected that this observation is probably a result of the fact that onset infers infinitesimal motion, when nonlinear dissipative processes are not yet strong.

IV. Test Approach

The purpose of the testing effort is to confirm that the standpipes on the main steam lines are not excited at power levels between CLTP and EPU conditions. To do so, a 1.0/5.87 scaled test facility was constructed that represents two of the main steam lines at SSES, from the steam dome to past the standpipes. However, only one main steam line was tested at a time.

4.1 Test Design

An examination of the main steam line geometry enables evaluation of the most representative steam line at SSES. Previous work by Ziada [10] suggests that the Strouhal number is strongly dependent on the distance from the last upstream elbow to the standpipe. An examination of available SSES drawings provides the distance summary shown in Table 4.1. The closest standpipe at SSES is on main steam line B. For this reason the valves were positioned as if on this main steam line. A 1.0/5.87 scale model of main steam line B was developed principally from drawing numbers FCIP-51-2953-1 (MSL A), FCI-P51-2952 (MSL B), and FCIP-51-2951-1 (MSL C and D) previously supplied by Susquehanna, and is shown schematically in Figure 4.1.

From drawings, pictures, and additional information supplied by PPL, an approximate cross-sectional area of the Crosby valve – as a function of distance from the main steam line – was generated. This cross-section includes the Sweepolet inlet, standpipe length and diameter, mating flange to the valve, and internal valve geometry to the closed end of the valve. The scaled configuration is shown in Figure 4.2.

4.2 Pre-Test Predictions

An acoustic model of the standpipe/valve combination was used to make pre-test predictions of the excitation frequency (single standpipe/valve combinations). These predictions are shown in Table 4.2.

Table 4.1. Standpipe location summary at SSES.

Main Steam Line	Distances From Upstream Elbow (ft)
A	Dead-Headed Branch Line
B	3.33, 7.50, and 11.50
C	3.46, 7.63, and 12.86
D	Dead-Headed Branch Line

Table 4.2. Pre-test predictions of excitation frequency and onset velocity.

Configuration	Excitation Frequency (Hz)	Onset Velocity (ft/sec)
Crosby as built	217.3	253.7

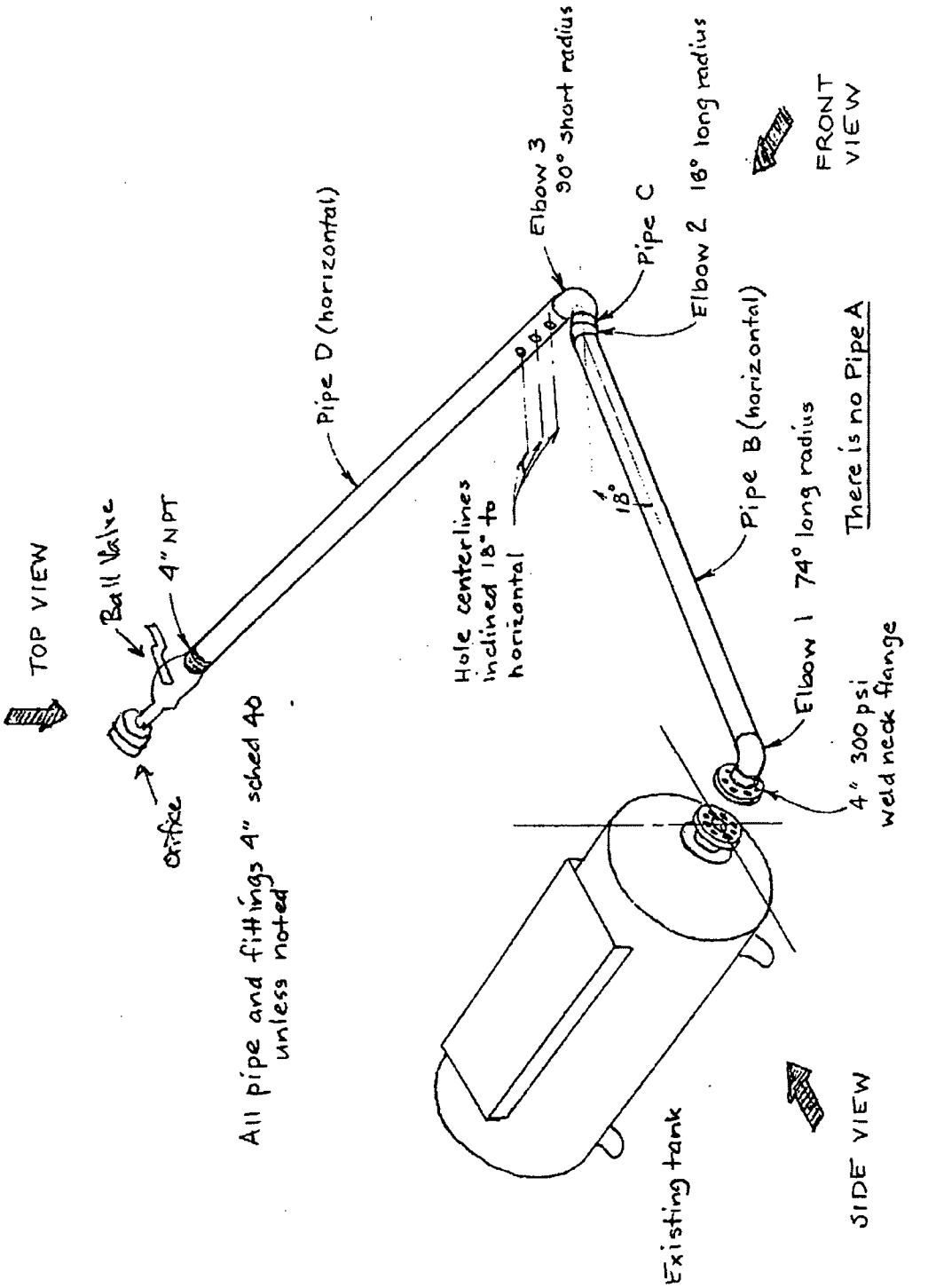

Figure 4.1. Schematic of SSES main steam line B. The tank is pressurized to 200 psig, then the ball valve is opened and flow ensues through the system. The orifice plate sets the Mach number in the pipe.

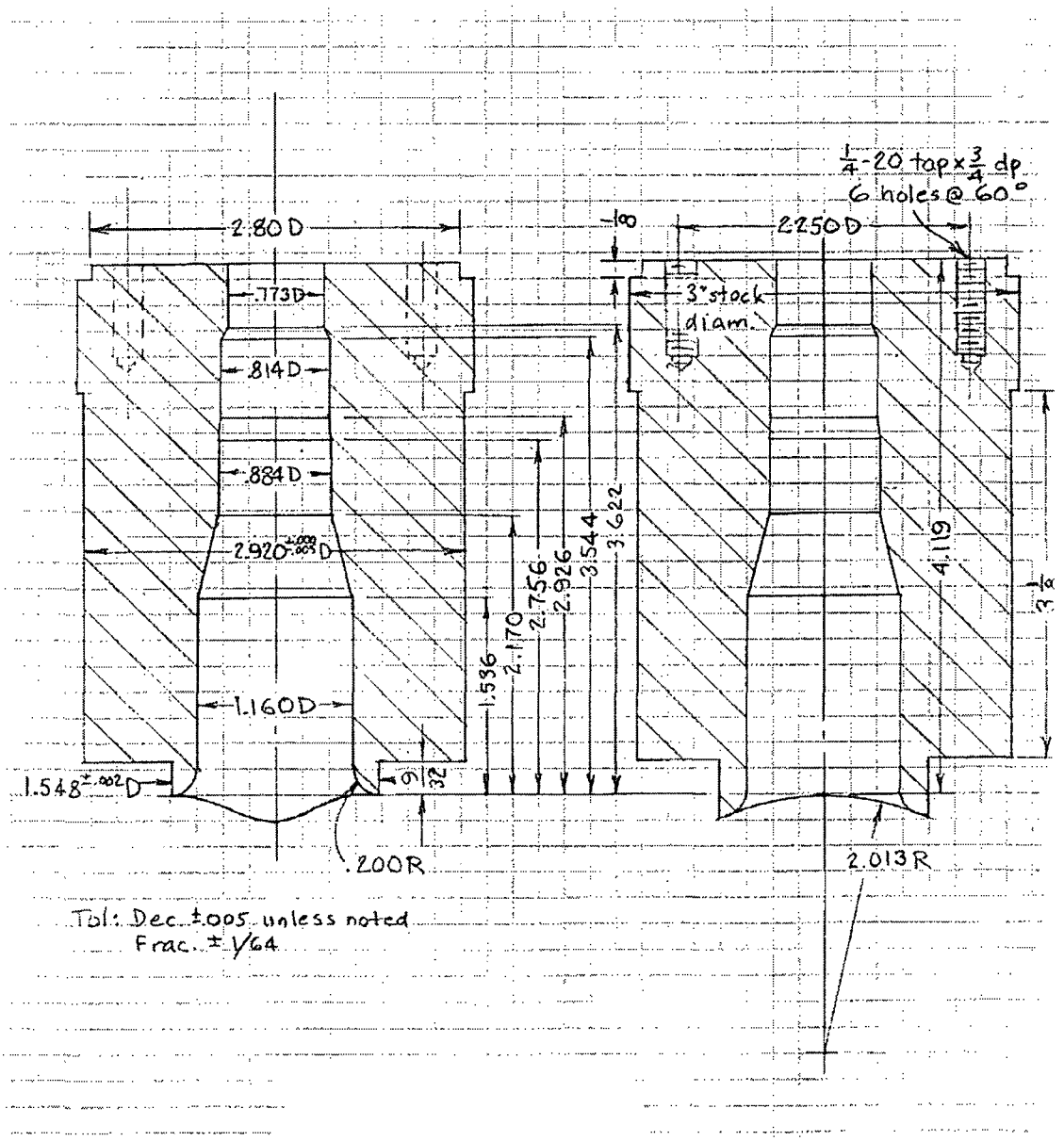

Figure 4.2. Cross-section of scaled standpipe and Crosby valve (all dimensions are in inches).

4.3 Dead-Headed Branch Lines

SSES main steam lines A and D position five standpipe/valves on dead-headed branch lines. To investigate FIV of this configuration, a second subscale steam line was constructed, as shown in Figure 4.3. Here the standpipe/valves were not expected to contribute significantly to the quarter wave frequency of the dead-headed branch line, and were therefore fabricated by pipes of the same diameter as the standpipes, but with a length that would recover the excitation frequency of the standpipe/valve combination as given in Table 4.2. As the branch lines are both approximately 24.0 feet in length (line A is 24.12 ft, while line B is 24.21 ft), the quarter standing wave frequency at full scale (Equation 3.2) is 16.6 Hz (for an acoustic speed of 1609 ft/sec). An acoustic circuit model of the dead-headed branch line with the five standpipes actually predicted a quarter standing wave frequency of 16.4 Hz. The purpose of testing is to determine if measured amplitudes in this line are a function of power level between CLTP and EPU operating conditions.

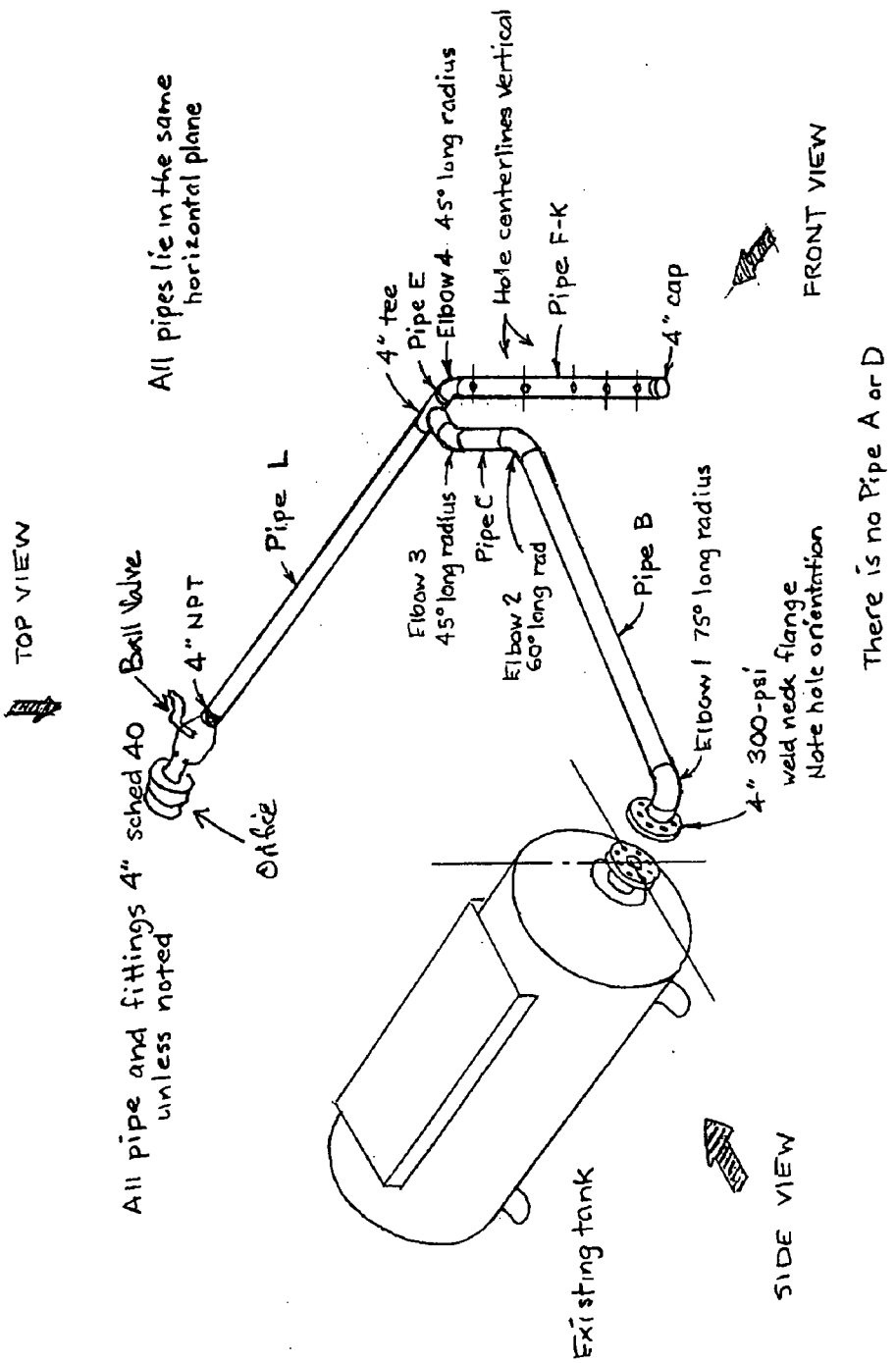

Figure 4.3. Schematic of SSES main steam lines A and D. The tank is pressurized to 200 psig, then the ball valve is opened and flow ensues through the system. The orifice plate sets the Mach number in the pipe.

V. Test Apparatus and Instrumentation

Test apparatus for the PPL testing program (Figure 5.1) consists of a pressure tank, a system of pipes to model full scale steam lines, a set of interchangeable model pressure relief valves, a ball valve, and a set of interchangeable orifices.

5.1 Experimental Facility

The test apparatus was assembled in the C.D.I. laboratory (Figures 5.2 and 5.3). The tank is a 250 gallon steel pressure vessel that was hydro tested to 300 psig. The piping is 4 inch Schedule 40 steel pipe with welded seams, flanged to the tank. The valve models were fabricated from PVC blocks, to replicate the standpipe and the valve geometry tested. A cross-sectional sketch of the subscale standpipe/valve configuration used in the study was shown previously in Figure 4.2.

The sizes on the orifices were selected so as to achieve the Mach numbers desired in the test (see Section 5.2). CLTP and EPU specific plant conditions correspond to main steam line Mach numbers of 0.0872 and 0.0999, respectively.

The system is charged from a Champion MNPL30A two-stage compressor, 10 HP, 250 psig maximum, with 37.3 CFM displacement.

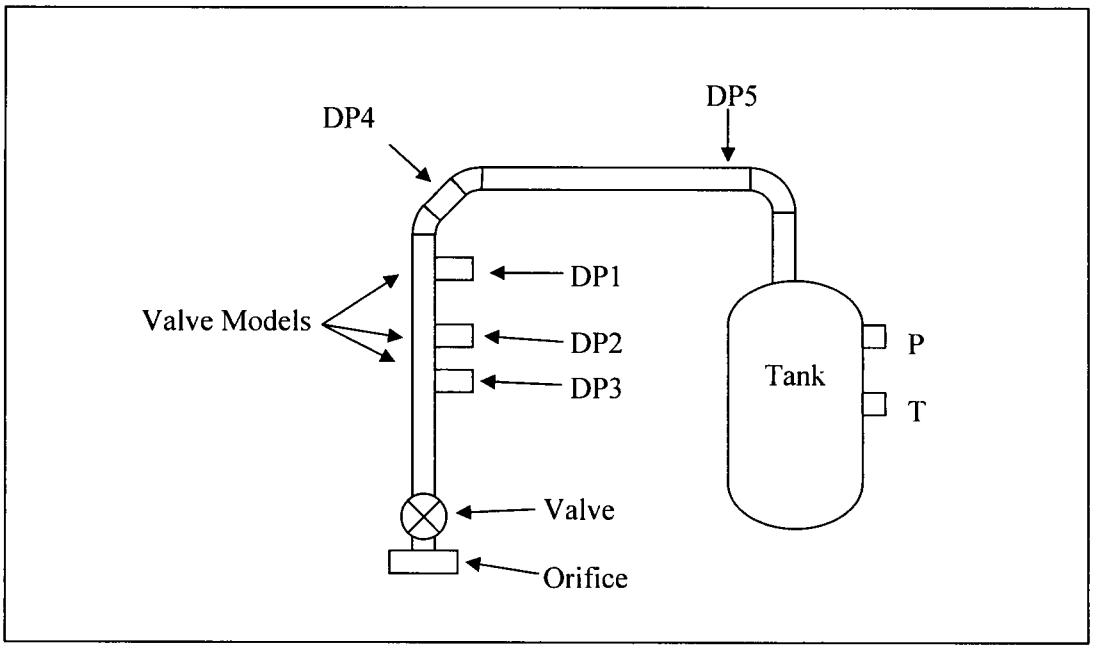

Figure 5.1. Schematic of test apparatus, where P is static pressure, T is temperature, and DP1 to DP5 are unsteady pressure transducers.

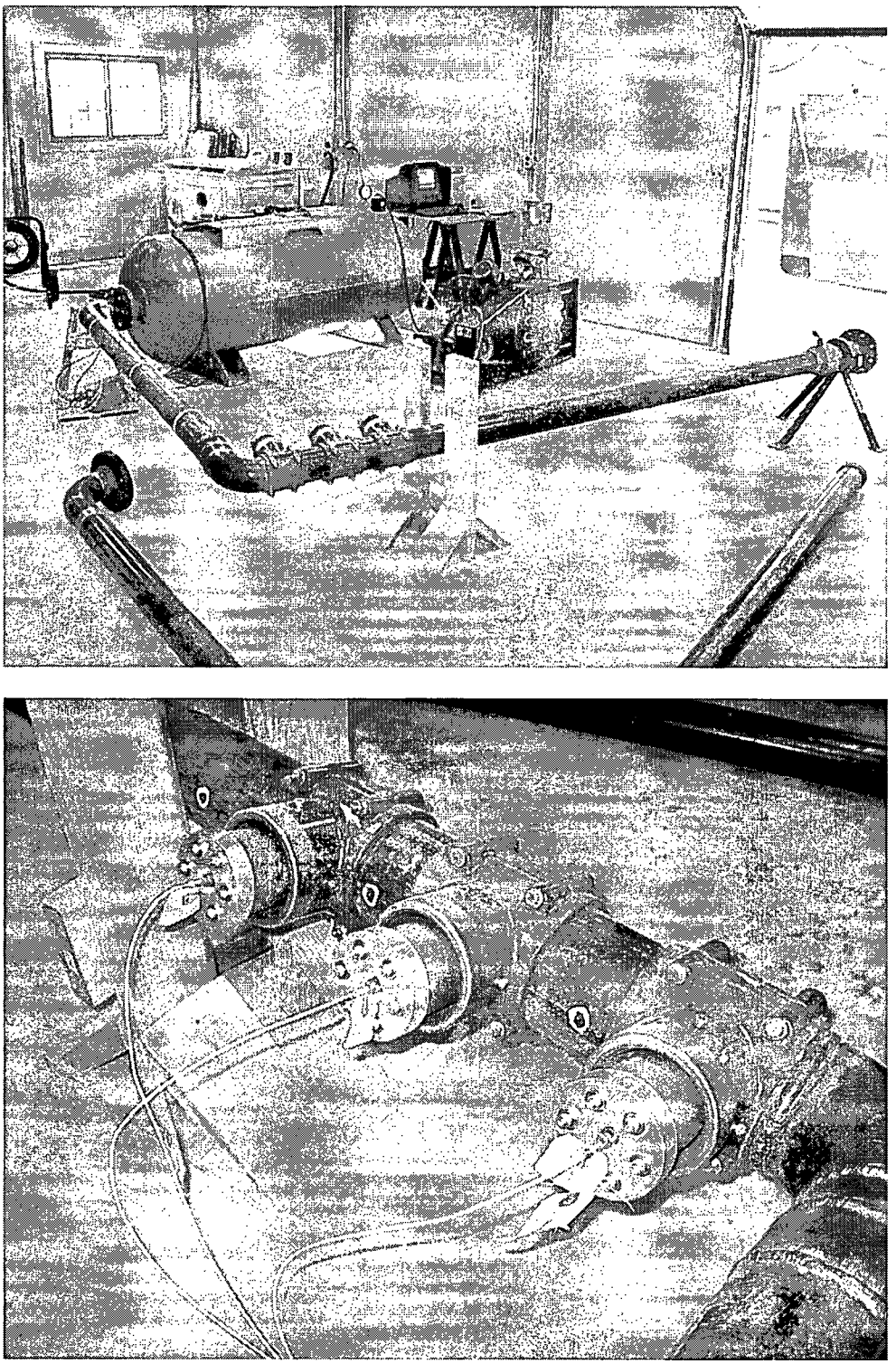

Figure 5.2. Photographs of the SSES blowdown facility: entire scaled main steam line B (top); the three standpipe locations (bottom).

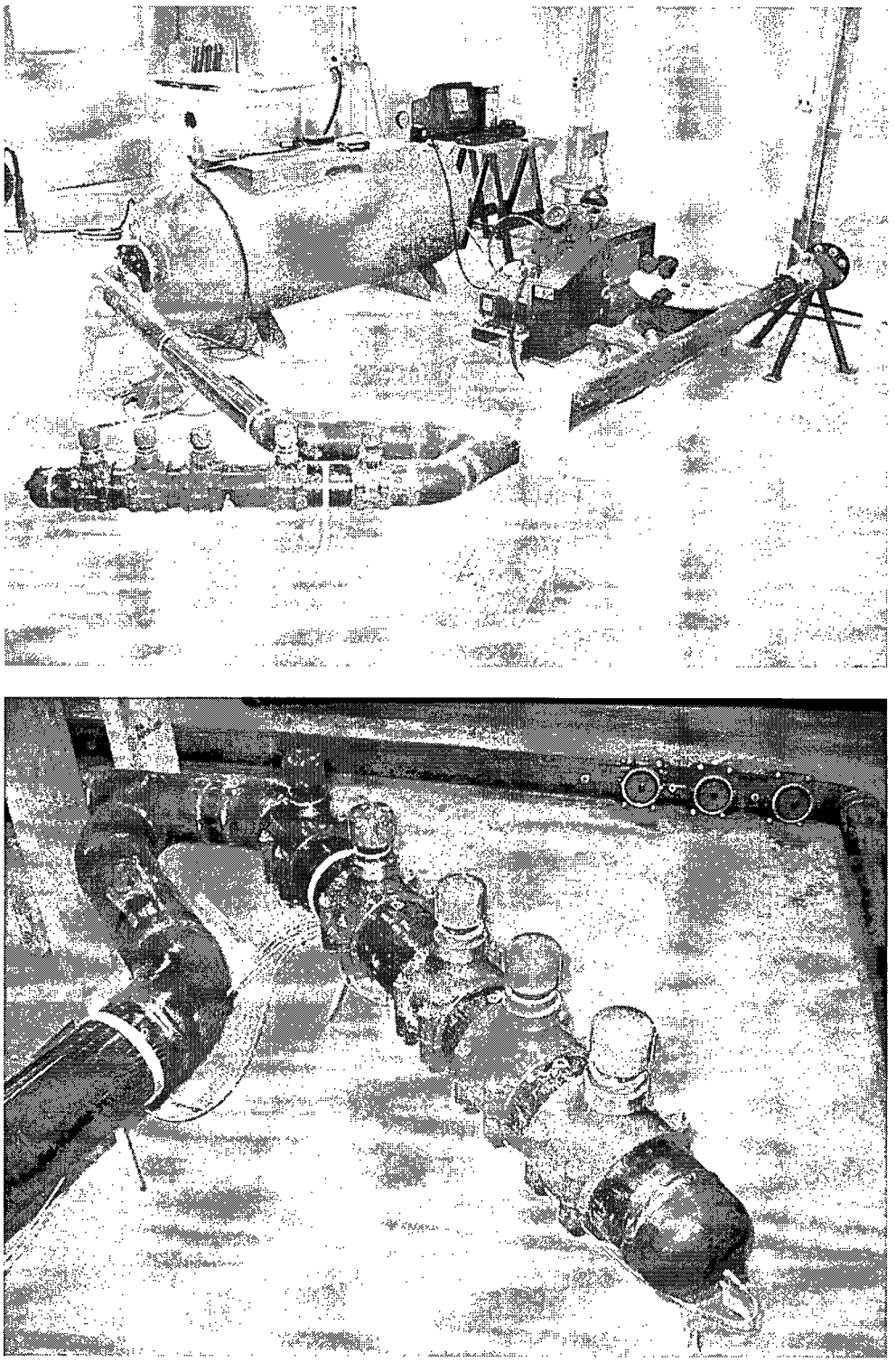

Figure 5.3. Photographs of the SSES blowdown facility: entire scaled main steam lines A and D (top); the dead-headed branch line (bottom).

5.2 Orifice Size

When the pressure in the tank is sufficiently high, the flow will be choked at the orifice and the Mach number in the pipe can be determined by using an assumption of compressible isentropic flow. It may be shown [14] that

$$\frac{A}{A^*} = \frac{1}{M}\left[\left(\frac{2}{\gamma+1}\right)\left(1+\frac{\gamma-1}{2}M^2\right)\right]^{\frac{\gamma+1}{2(\gamma-1)}} \tag{5.1}$$

where A is the area of the pipe, A* is the effective area of the orifice, M is the Mach number, and γ is the ratio of specific heats, equal to 1.4 for air. The effective area of the orifice is equal to the discharge coefficient C_D times the actual orifice area. The value of C_D for the present effort is 0.85 [15], so that $A^* = C_D A_a$, where A_a is the actual area of the orifice.

The relationship between orifice diameter and Mach number is shown in Figure 5.4. The Mach numbers at CLTP and EPU (0.0872 and 0.0999, respectively) were obtained from specific plant conditions supplied by PPL at these two full-scale power settings, with an acoustic speed of 1609 ft/sec.

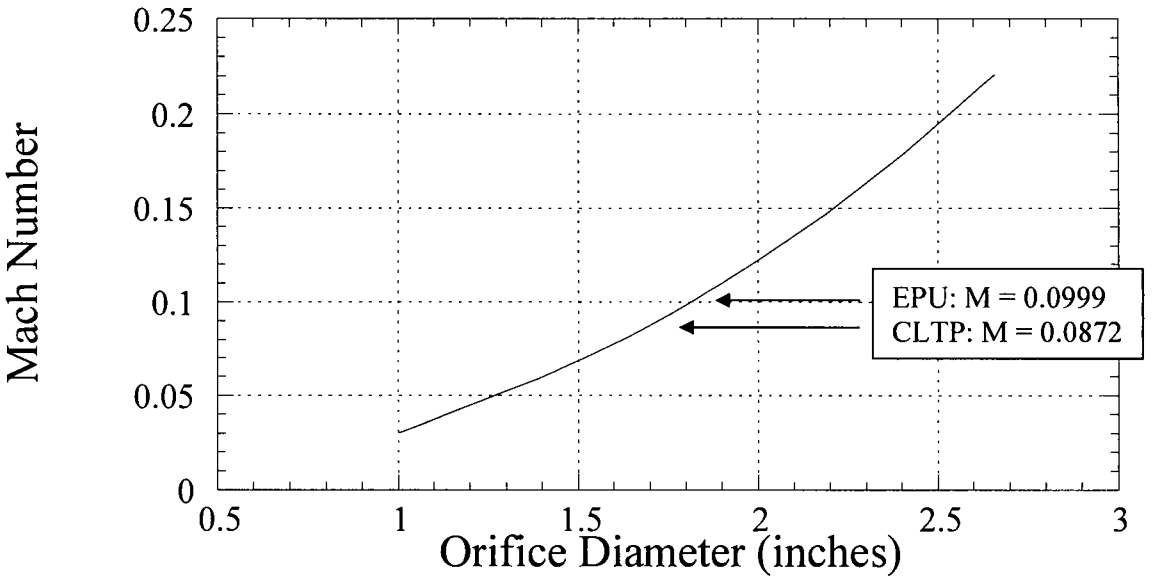

Figure 5.4. Behavior of Mach number with orifice size.

Table 5.1 tabulates the physical orifice diameters tested, steam line Mach numbers, and plant power levels as a percentage of EPU power.

Table 5.1. Plant power and main steam line (MSL) Mach numbers, where the CLTP Mach number = 0.0872 and the EPU Mach number = 0.0999.

Orifice Diameter (inch)	MSL Mach Number	% EPU Power
1.003	0.0302	30.2
1.270	0.0487	48.7
1.390	0.0585	58.6
1.510	0.0690	69.1
1.630	0.0805	80.6
1.724	0.0901	90.2
1.812	0.0996	99.7
1.854	0.1044	104.5
1.899	0.1096	109.7
2.000	0.1218	121.9
2.087	0.1329	133.0
2.187	0.1462	146.3
2.400	0.1772	177.4
2.657	0.2194	219.6

5.3 Instrumentation and Data Acquisition

The test apparatus is fitted with transducers to measure static pressure in the tank, temperature in the tank, unsteady pressure at the three valve locations, and unsteady pressure at two additional locations directly on the line. A typical wiring diagram is shown in Figure 5.5.

Voltage signals from the various instruments are sampled by a Cyber Research CMF 3202DA A/D board. The board resides in an eMachines T3882 PC running Microsoft Windows XP and a custom A/D application.

Static pressure measurements are provided by an Omega PX302-200GV pressure transducer (CDI 0568) powered by an Omega PSS-10 10 volt power supply. The output voltage is fed to a differential channel on the A/D system.

Temperature is measured by an Omega thermocouple (CDI 0545) powered by an Omega High Performance Temperature Indicator DP41-TC display unit (CDI 0544). The display unit samples and conditions the thermocouple signal and produces a voltage suitable for a differential channel of the A/D system. Since the sampling rate of the display unit is less than the sampling rate of the A/D system, a trace of the temperature signal captured by the A/D system displays a "staircase" effect during blowdown when the temperature changes rapidly.

Unsteady pressures, whether measured at the top of the model valves or directly on the piping system, are provided by Kistler Piezotron Pressure Transducers Model 211B4 (CDI 0011, 0012, 0013, 0014, and 0015), via a four-channel Kistler Power Supply/Signal Conditioner Type 5134 (CDI 0495) and a Sunstrand Piezotron Coupler signal conditioner (CDI 0024).

Connections between the A/D system and the pressure transducer, the temperature display, and the unsteady pressure signal conditioners are configured the same way for all tests. Connections between the unsteady pressure transducers and their signal conditioners vary according to valve installation.

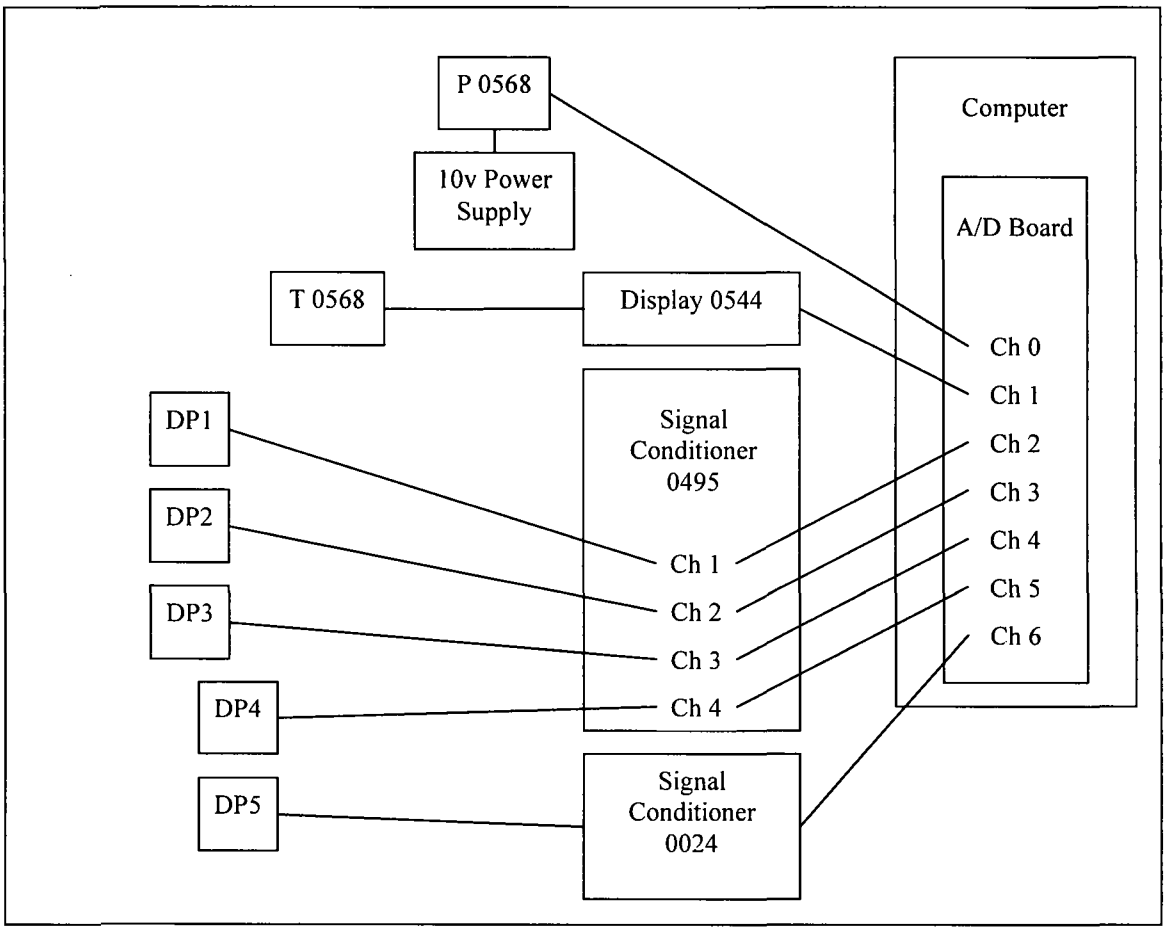

Figure 5.5. Schematic of data acquisition system with five DP transducers

VI. Test Matrix

The test matrix is summarized in Table 6.1.

Table 6.1. Test matrix. Main steam line B/C tests are identified by three letters (X, Y, Z), where X corresponds to the upstream valve, Y corresponds to the middle valve, and Z corresponds to the downstream valve (see Figure 5.1). Main steam line A/D tests are identified by two pressure transducers on the dead-headed branch line. Terminology: CR = Crosby valve; DPE = pressure transducer at the end of the dead-headed branch line; DPM = pressure transducer at the middle of the dead-headed branch line.

Test	Date	Orifice (inch)	Notes
BC Test 1	12/15/05	1.510	CR, CR, CR
BC Test 2	12/15/05	1.510	CR, CR, CR
BC Test 3	12/15/05	1.854	CR, CR, CR
BC Test 4	12/15/05	1.854	CR, CR, CR
BC Test 5	12/15/05	1.854	CR, CR, CR
BC Test 6	12/15/05	1.854	CR, CR, CR
BC Test 7	12/15/05	2.657	CR, CR, CR
BC Test 8	12/15/05	2.657	CR, CR, CR
BC Test 9	12/15/05	1.630	CR, CR, CR
BC Test 10	12/15/05	1.724 (1)	CR, CR, CR
BC Test 11	12/15/05	1.812 (2)	CR, CR, CR
BC Test 12	12/15/05	2.000	CR, CR, CR
BC Test 13	12/15/05	2.087	CR, CR, CR
BC Test 14	12/15/05	2.187	CR, CR, CR
BC Test 15	12/15/05	2.400	CR, CR, CR
AD Test 1	12/22/05	2.657	DPE, DPM
AD Test 2	12/22/05	1.003	DPE, DPM
AD Test 3	12/22/05	1.003	DPE, DPM
AD Test 4	12/22/05	1.854	DPE, DPM
AD Test 5	12/22/05	1.854	DPE, DPM
AD Test 6	12/22/05	1.854	DPE, DPM
AD Test 7	12/22/05	1.510	DPE, DPM
AD Test 8	12/22/05	1.630	DPE, DPM
AD Test 9	12/22/05	1.812 (2)	DPE, DPM
AD Test 10	12/22/05	2.000	DPE, DPM
AD Test 11	12/22/05	2.087	DPE, DPM
AD Test 12	12/22/05	2.187	DPE, DPM
AD Test 13	12/22/05	2.400	DPE, DPM
AD Test 14	12/22/05	2.657	DPE, DPM

Tests denoted with (1) indicate an orifice size approximating CLTP conditions.
Tests denoted with (2) indicate an orifice size approximating EPU conditions.

VII. Test Procedure

7.1 Data Collection

For each run, the tank is pressurized with air to a static pressure of approximately 200 psig. A custom computer program for A/D collection is started and commands the A/D board inside to begin collecting data for a period of 15 seconds. Signals on all connected channels are collected at a rate of 4000 samples/second/channel and stored in a disk file. Immediately following the start of data collection, the ball valve near the orifice is opened quickly, and the pressurized air in the tank and the piping system escapes through the orifice until equilibrium with atmospheric pressure is achieved. The pressure time history data are stored in a data file for subsequent analysis.

7.2 Data Reduction

The data reduction procedure to reduce measured pressured fluctuations to normalized power spectral density (PSD) results is now described. Raw pressure measurements from pressure transducers in the standpipes are high-pass filtered to remove the slow transient associated with the change in system (total) pressure. A third-order Butterworth filter with cutoff frequency of 2 Hz is used here. The data are processed using a forward-reverse filtering technique resulting in zero phase shift and sixth-order roll-off characteristics in the stop band. The filtered pressure fluctuations are normalized by the dynamic pressure at CLTP, which is derived from measurement in the reservoir (total) pressure and the flow Mach number. The total pressure is low-pass filtered, with cutoff frequency of 2 Hz, to remove high frequency noise, using a similar technique for the standpipe pressure sensors. Time histories of normalized pressure fluctuations are used to estimate the PSD for each transducer, which is determined using Welch's averaged periodogram method. The normalized pressure fluctuations are separated into 400-point (100-msec) overlapping blocks that are de-trended and windowed using a Hanning weighting to reduce side-lobe leakage in the PSD estimate. This approach provides PSD estimates with frequency resolution of 10 Hz with maximum Nyquist frequency of 2000 Hz (sampling rate was 4000 Hz). A MatLab (Version 6.5 Release 13, from The MathWorks, Inc.) program is used for data reduction.

A typical pressure time history in the tank is shown in Figure 7.1. Resulting normalized PSD plots for all tests are shown in Appendix A.

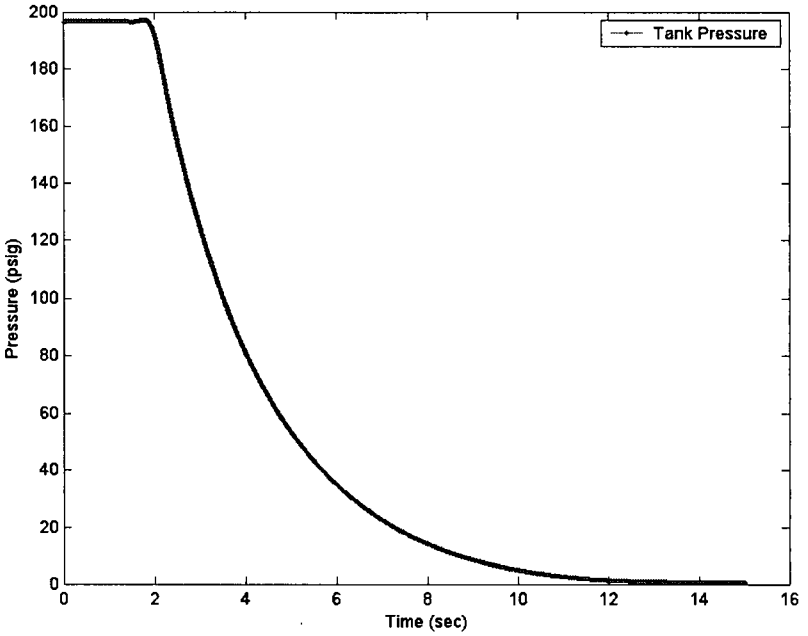

Figure 7.1. Stagnation pressure time history.

VIII. Results

The purpose of the PPL study was to characterize the behavior of the standpipe/valve combination currently at SSES. To this end, the results of the numerous tests conducted by C.D.I. may be examined with regard to excitation frequency, Mach number, onset velocity, and dead-headed branch line effects.

8.1 Excitation Frequency

A comparison of measured excitation frequencies (frequencies where peaks in the PSDs are recorded in the subscale experiments) with pre-test predictions (from Table 4.3) is shown in Table 8.1. The predicted excitation frequency is based on a single standpipe/valve, while the full-scale excitation frequency is obtained by averaging all measured excitation frequency data taken for the standpipe/valve combinations tested, as summarized in Table 6.1, and scaling to full scale (by multiplying the measured excitation frequency by 0.2478). These results suggest a close agreement between experimental results and theoretical predictions.

Table 8.1. Comparison between predicted and measured excitation frequencies for SSES.

Configuration	Predicted Excitation Frequency (Hz)	Measured Excitation Frequency (Hz)	Full-Scale Excitation Frequency (Hz)
Crosby as built	217.3	875.2	218.1

8.2 Mach Number

The PSD results shown in Appendix A provide a good indication of peak response for standpipe/valve behavior at specific Mach numbers. However, a better metric is the root mean square (RMS) of the recorded signal. This parameter was determined by integrating the PSD from 100 to 1000 Hz, then taking the square root to recover the RMS pressure level. These results will now be examined.

The subscale tests swept Mach number by changing orifice size (increasing orifice size to increase Mach number as seen in Figure 5.4). The effect of Mach number on maximum normalized RMS pressure may be seen in Figure 8.1. The curve shown here includes (for Mach numbers between 0.07 and 0.15) a double vortex mode, followed (for Mach numbers between 0.15 and above) by a single vortex mode (vortex mode nomenclature is discussed in [11]). The double vortex mode is reminiscent of the Strouhal curve, shown in Figure 3.2. It may be seen that the EPU Mach number (0.1050) is near the peak pressure for the double vortex mode excitation of the standpipe/valve.

The double vortex mode peaks at a Mach number of approximately 0.11. It has been suggested in [12] that the peak pressure in the double vortex mode should be at least one order of magnitude lower than the peak pressure in the single vortex mode. Figure 8.1 shows that the single vortex mode peak was not reached in the tests, although the figure does suggest that the

double vortex mode peak will be at least a factor of eight smaller that the single vortex mode peak. It would appear prudent for PPL to check whether any pressure oscillations in the main steam lines were observed at frequencies above 200 Hz, at or above CLTP conditions.

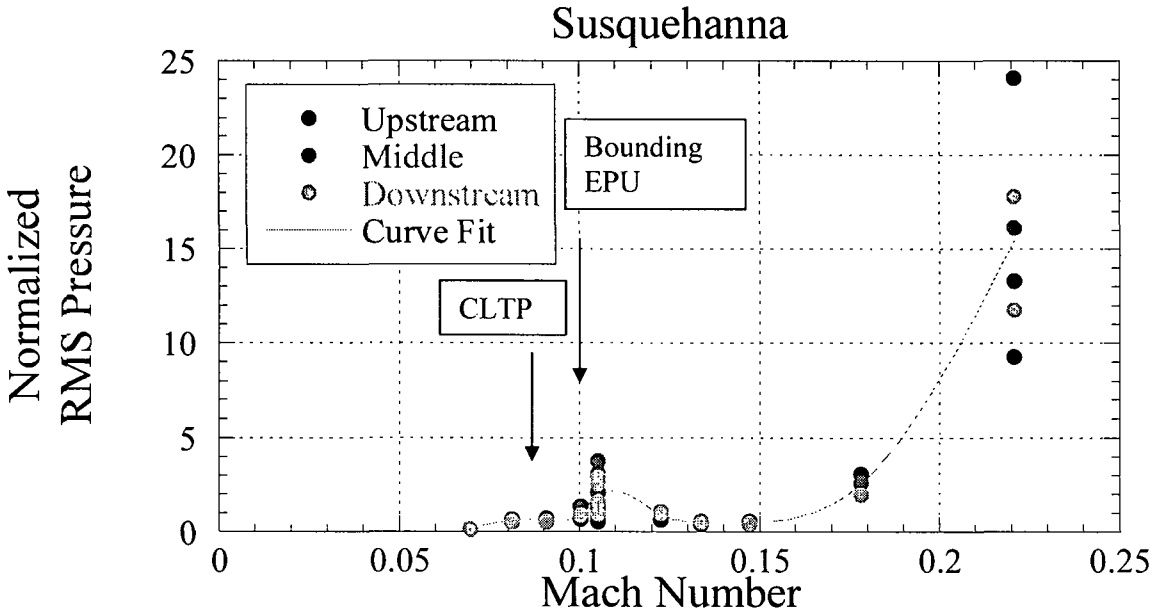

Figure 8.1. Normalized RMS pressure for all B/C tests: upstream refers to the pressure at the upstream standpipe/valve; middle refers to the pressure at the middle standpipe/valve; and downstream refers to the pressure at the downstream standpipe/valve. A cubic spline curve fit to all data is shown by the green curve.

8.3 Onset Velocity

If onset is defined as the point at which the normalized RMS pressure is ten percent of the maximum normalized RMS pressure measured (in this case 24.0 from Figure 8.1), a Mach number of 0.18 should be near onset (even though the pressure curve peak was not measured in the subscale tests). Table 8.2 compares the predicted and measured onset velocities based on these assumptions.

Table 8.2. Comparison between predicted and measured onset velocities for SSES.

Configuration	Predicted Onset Velocity (ft/sec)	Measured Onset Velocity (ft/sec)
Crosby as built	253.7	289.6

8.4 Dead-Headed Branch Line Effects

The dead-headed branch line results are also shown in Appendix A. These results suggest that the dead-headed branch line will contribute a source in the main steam line, specifically above a Mach number of 0.0810 (Figure 8.2). This figure indicates that the normalized RMS pressures between CLTP and EPU conditions are increasing slowly with Mach number. Therefore, in this frequency range, pressure fluctuations are anticipated to increase as the square of the flow velocity between CLTP and EPU conditions. The frequency comparison is shown in Table 8.3.

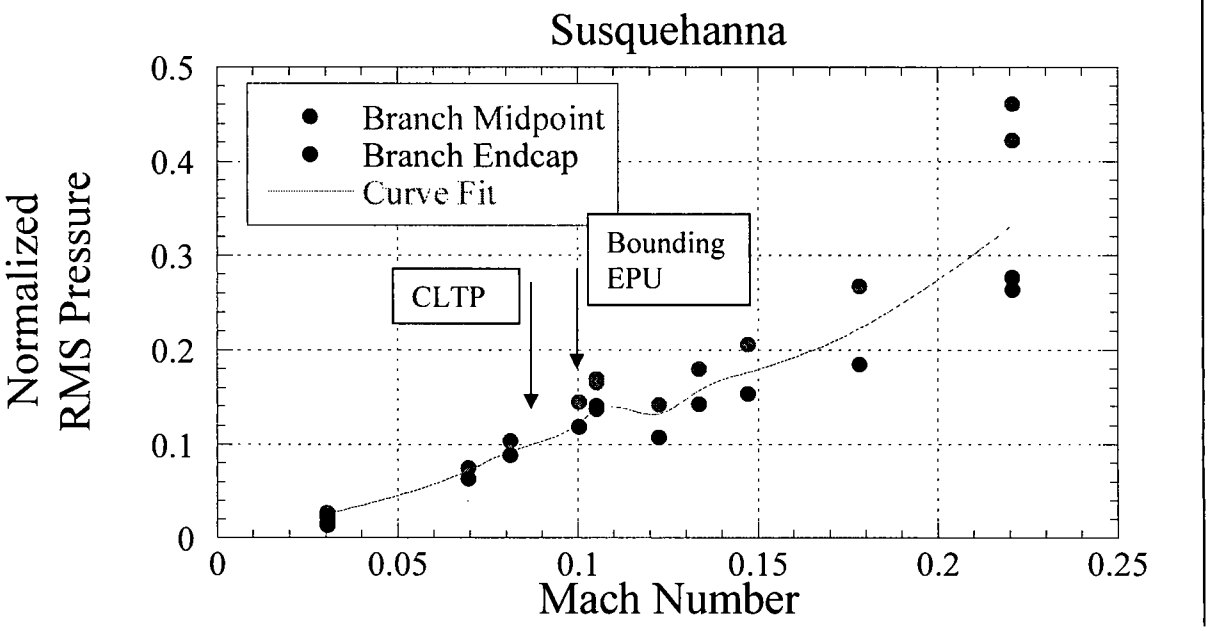

Figure 8.2. Normalized RMS pressure for all A/D tests: branch endcap refers to the pressure at the end of the dead-headed branch line; and branch midpoint refers to the pressure at the middle of the dead-headed branch line. A cubic spline curve fit to all data is shown by the green curve.

Table 8.3. Comparison between predicted and measured excitation frequency for the dead-headed branch lines for SSES.

Configuration	Predicted Excitation Frequency (Hz)	Measured Excitation Frequency (Hz)	Full-Scale Excitation Frequency (Hz)
Dead-headed branch lines as built	16.4	60.0	15.0

IX. Conclusions

Normalized acoustic RMS pressures from dead-headed branch lines and from standpipes for the Crosby safety valves do not increase in amplitude as power is increased from CLTP to EPU conditions in the SSES plant. It is therefore anticipated that unsteady dryer loads are expected to increase from CLTP to EPU conditions as the flow velocity squared. Curiously, the plant is currently operating at CLTP, where FIV is anticipated from the relief valve standpipes at a frequency of 218 Hz. In-plant measurements if undertaken should be sampled at a high enough digitization rate to determine whether this load is present.

X. Quality Assurance

All quality-related activities will be performed in accordance with the C.D.I. Quality Assurance Manual, Revision 13 [16]. Quality-related activities are those activities which will be directly related to the planning, execution, and objectives of the test program. Supporting activities, such as test apparatus design, fabrication, and assembly, are not controlled by the C.D.I. Quality Assurance Manual. C.D.I.'s Quality Assurance Program provides for compliance with the reporting requirements of 10 CFR Part 21. All instrument certifications, calibrations, test procedures, data reduction procedures, and test results will be contained in a Design Record File kept on file at C.D.I. offices.

XI. References

1. Continuum Dynamics, Inc. 2005. Hydrodynamic Loads on Susquehanna Unit 2 Steam Dryer to 200 Hz. C.D.I. Report No. 05-16.

2. Continuum Dynamics, Inc. 2005. Evaluation of Continuum Dynamics, Inc. Steam Dryer Load Methodology Against Quad Cities Unit 2 In-Plant Data. C.D.I. Report No. 05-10.

3. Webb, M. and P. Ellenberger. 1995. Piping Retrofit Reduces Valve-Damaging Flow Vibration. *Power Engineering.*

4. Bernstein, M. D. and Bloomfield, W. J. 1989. Malfunction of Safety Valves Due to Flow Induced Vibration. *Flow-Induced Vibrations 1989* (ed: M. K. Au-Yang, S. S. Chen, S. Kaneko and R. Chilukuri) PVP 154: 155-164. New York: ASME.

5. Coffman, J. T. and Bernstein, M. D. 1980. Failure of Safety Valves Due to Flow Induced Vibration. *Transactions of the ASME* 102.

6. Continuum Dynamics, Inc. 2002. Mechanisms Resulting in Leakage from Main Steam Safety Valves. C.D.I. Technical Note No. 02-16. Final Report Prepared for Energy Northwest.

7. Continuum Dynamics, Inc. Letter Report to Susquehanna. November 17, 2005.

8. Chen, Y. N. and D. Florjancic. 1975. Vortex-Induced Resonance in a Pipe System due to Branching. *Proceedings of International Conference on Vibration and Noise in Pump, Fan and Compressor Installations* 79-86. University of Southampton, England.

9. Baldwin, R. M. and H. R. Simmons. 1986. Flow-Induced Vibration in Safety Relief Valves. *ASME Journal of Pressure Vessel Technology* 108: 267-272.

10. Ziada, S. and Shine, S. 1999. Strouhal Numbers of Flow-Excited Acoustic Resonance of Closed Side Branches. *Journal of Fluids and Structures* 13: 127-142.

11. Ziada, S. 1994. A Flow Visualization Study of Flow Acoustic Coupling at the Mouth of a Resonant Side-Branch. *Journals of Fluids and Structures* 8: 391-416.

12. Graf, H. R. and S. Ziada. 1992. Flow-Induced Acoustic Resonance in Closed Side Branches: An Experimental Determination of the Excitation Source. *Proceedings of ASME International Symposium on Flow-Induced Vibration and Noise, Vol. 7: Fundamental Aspects of Fluid-Structure Interactions* (ed: M. P. Paidoussis, T. Akylas and P. B. Abraham). AMD-Vol. 51: 63-80. New York: ASME.

13. Continuum Dynamics, Inc. 2004. Plant Unique Steam Dryer Loads to Support I&E Guidelines. C.D.I. Technical Memorandum No. 04-14.

14. Shapiro, A. H. 1953. The Dynamics and Thermodynamics of Compressible Fluid Flow. Volume I. John Wiley and Sons: New York, NY.

15. Kayser, J. C. and R. L. Shambaugh. 1991. Discharge Coefficients for Compressible Flow Through Small-Diameter Orifices and Convergent Nozzles. *Chemical Engineering Science* 46(7):1697-1711.

16. Continuum Dynamics, Inc. Quality Assurance Manual. Revision 13. June 2002.

Appendix A: Normalized PSD Results

Appendix A provides the normalized PSD traces for the pressure time histories taken during the test program. Here, normalized PSD is obtained by normalizing unsteady pressure by the dynamic pressure at CLTP, then constructing the PSD from the Fast Fourier transform.

The nomenclature on the B/C test plots (Figures A.1 to A.15) are:

Upstream	Unsteady pressure recorded at the valve end of the upstream standpipe/valve
Middle	Unsteady pressure recorded at the valve end of the middle standpipe/valve
Downstream	Unsteady pressure recorded at the valve end of the downstream standpipe/valve

The nomenclature on the A/D test plots (Figures A.16 to A.29) are:

Branch Midpoint	Unsteady pressure recorded at the center of the dead-headed branch line
Branch Endcap	Unsteady pressure recorded at the closed end of the dead-headed branch line

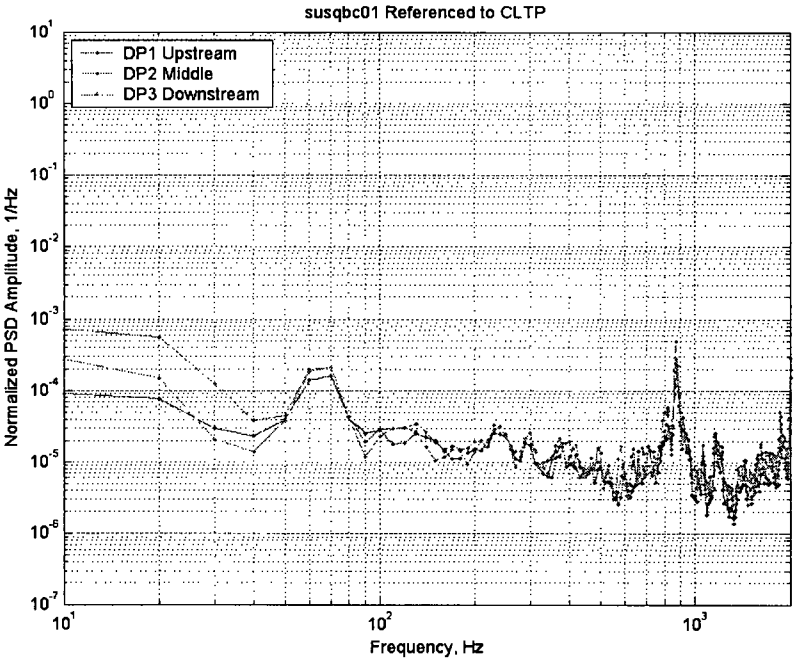

Figure A.1. Normalized PSD for B/C Test 1: Mach number = 0.0690.

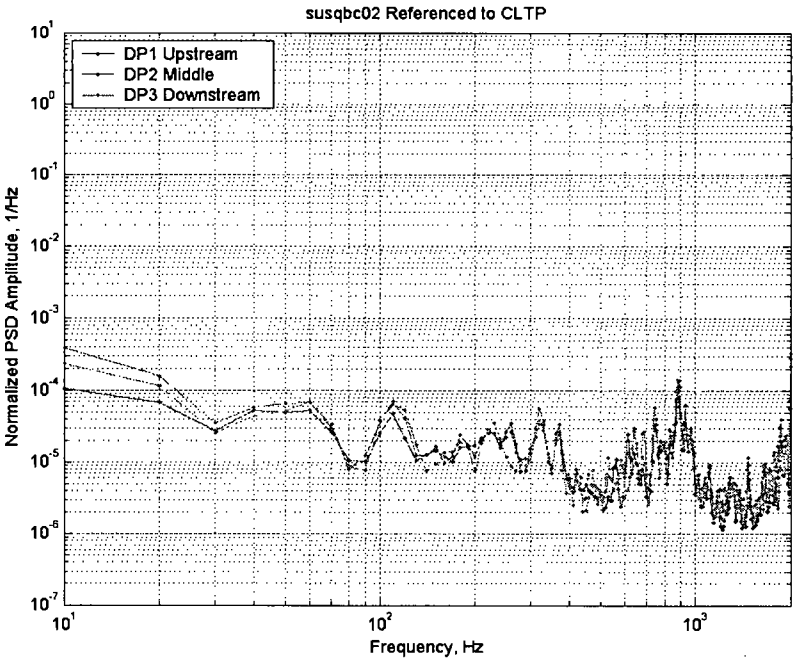

Figure A.2. Normalized PSD for B/C Test 2: Mach number = 0.0690.

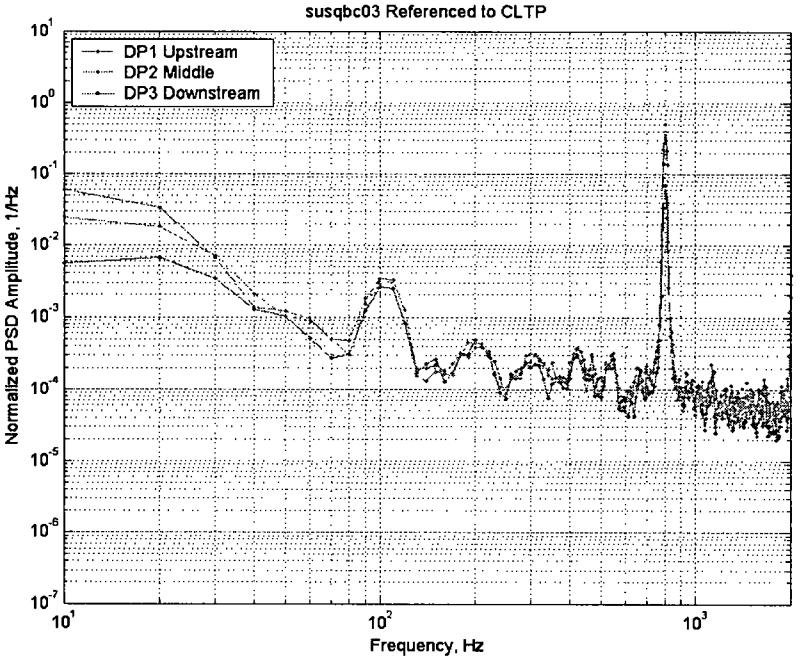

Figure A.3. Normalized PSD for B/C Test 3: Mach number = 0.1044.

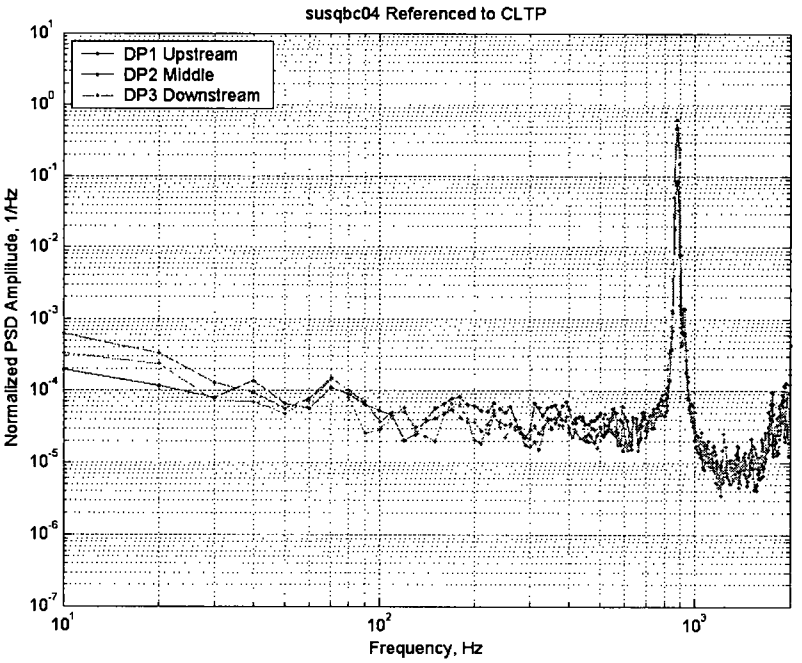

Figure A.4. Normalized PSD for B/C Test 4: Mach number = 0.1044.

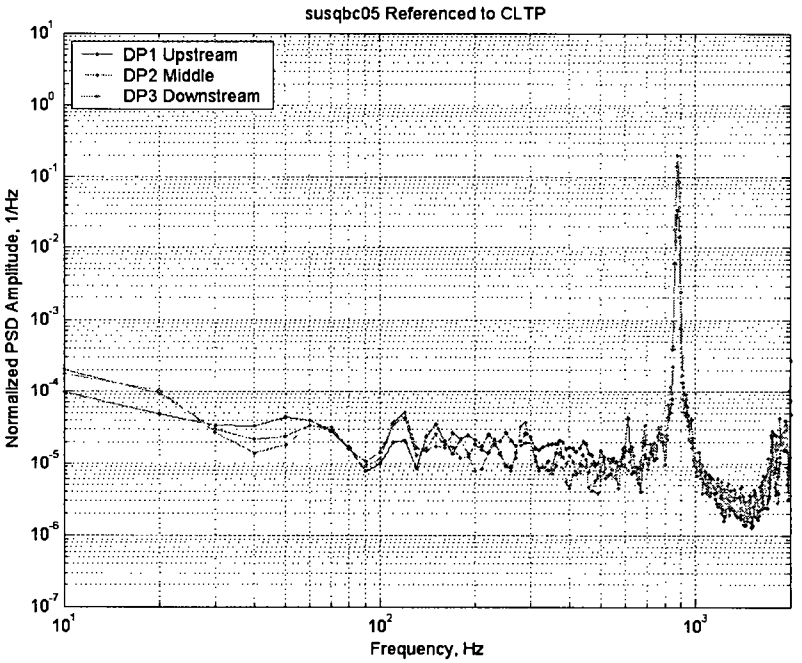

Figure A.5. Normalized PSD for B/C Test 5: Mach number = 0.1044.

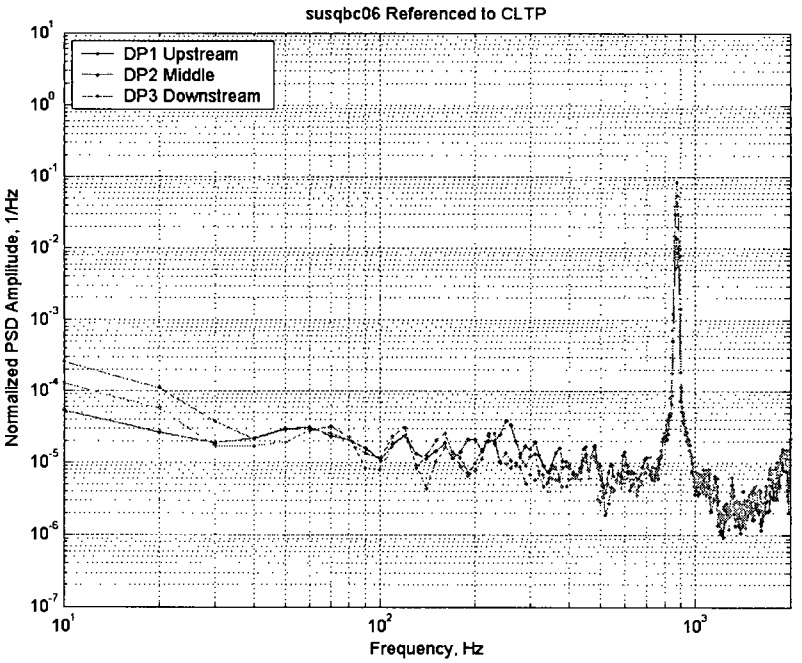

Figure A.6. Normalized PSD for B/C Test 6: Mach number = 0.1044.

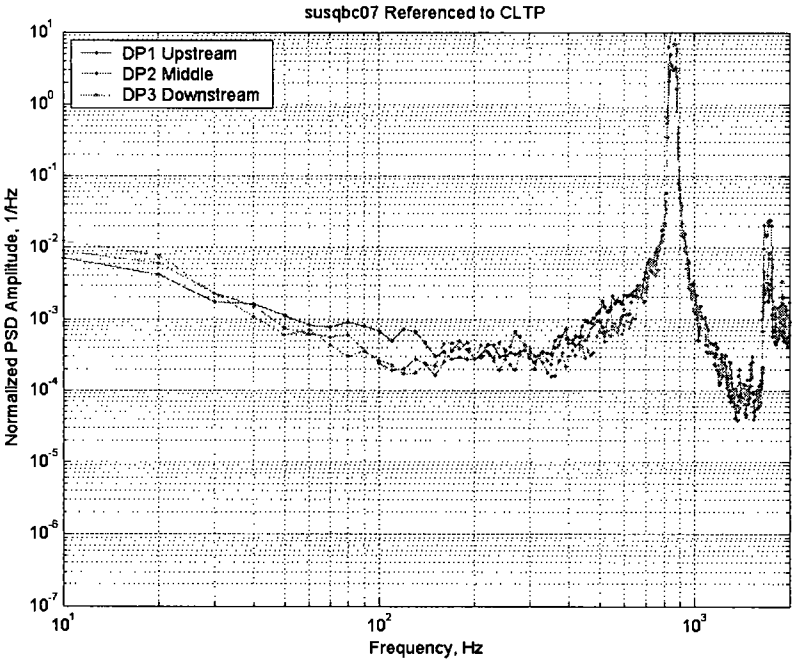

Figure A.7. Normalized PSD for B/C Test 7: Mach number = 0.2194.

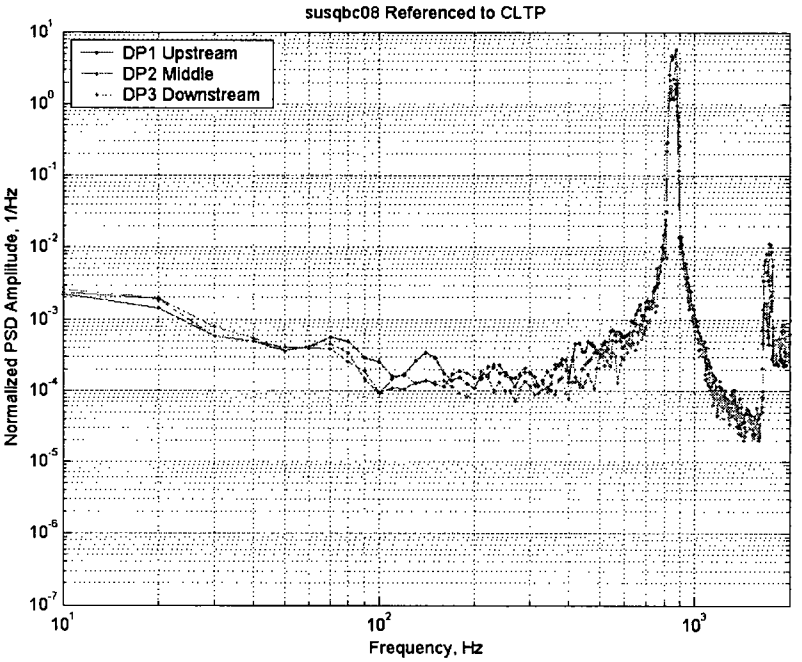

Figure A.8. Normalized PSD for B/C Test 8: Mach number = 0.2194.

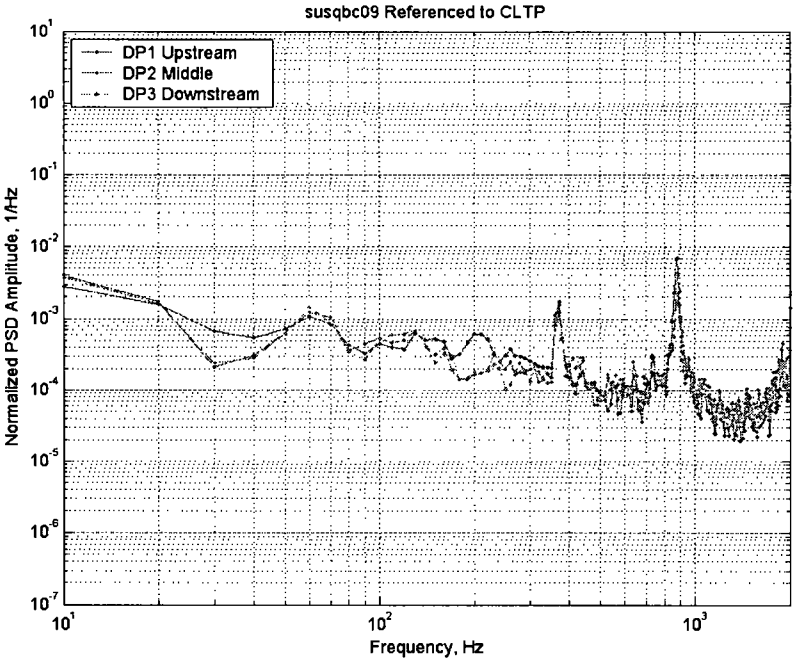

Figure A.9. Normalized PSD for B/C Test 9: Mach number = 0.0805.

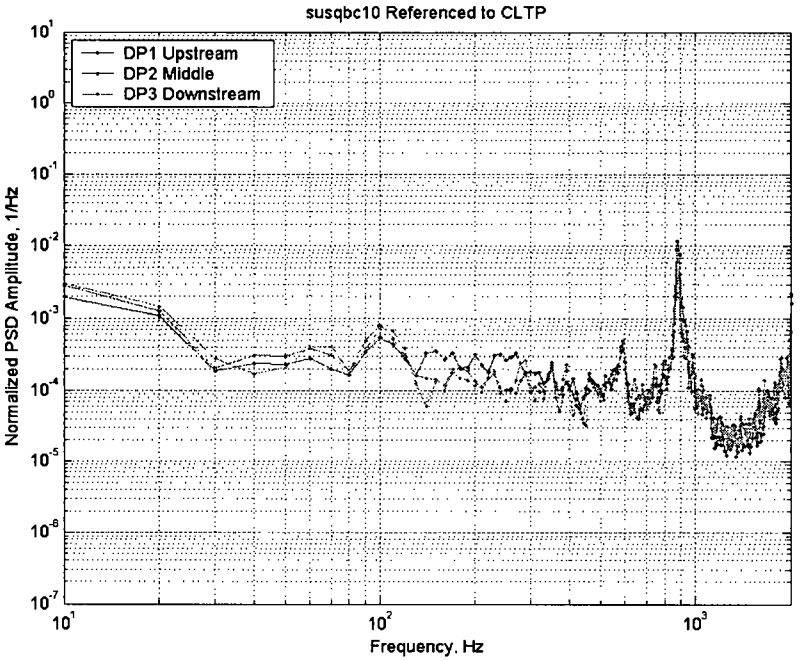

Figure A.10. Normalized PSD for B/C Test 10: Mach number = 0.0901.

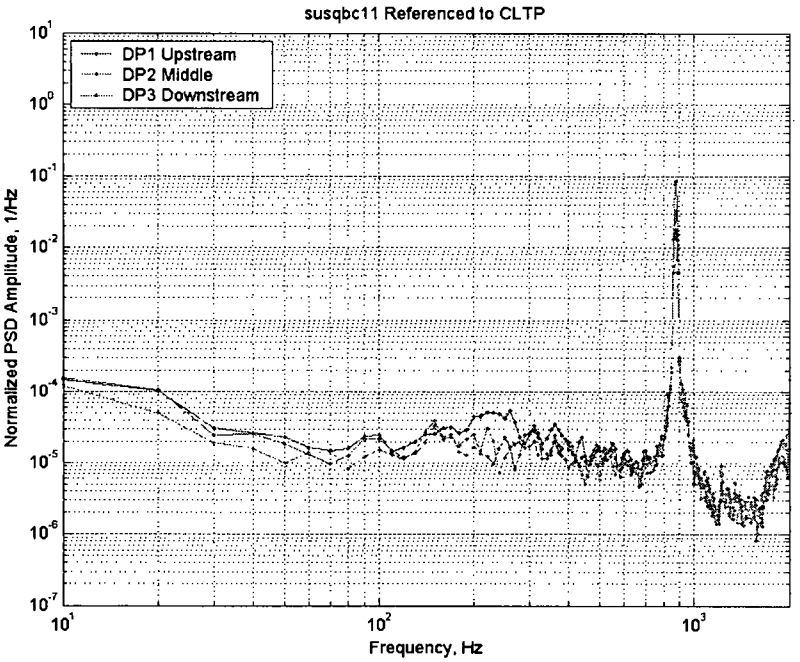

Figure A.11. Normalized PSD for B/C Test 11: Mach number = 0.0996.

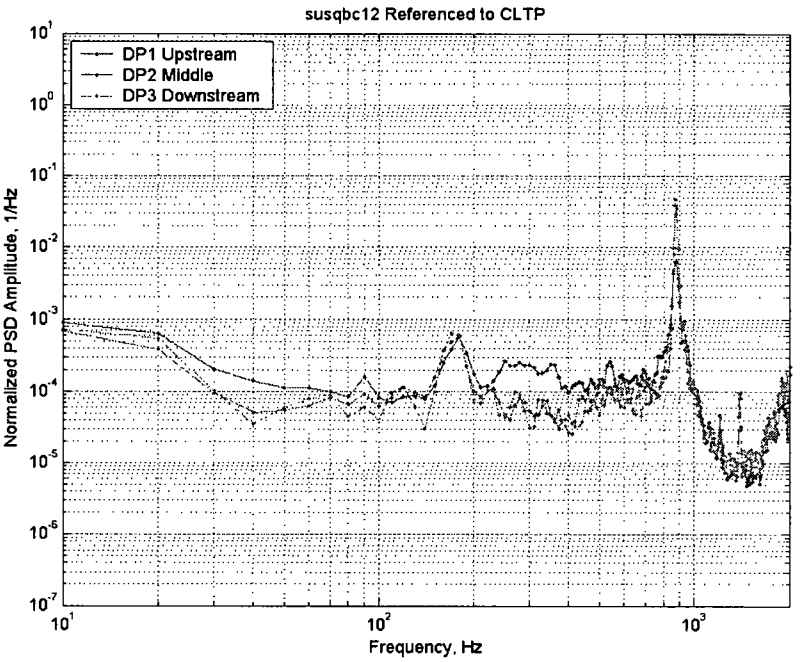

Figure A.12. Normalized PSD for B/C Test 12: Mach number = 0.1218.

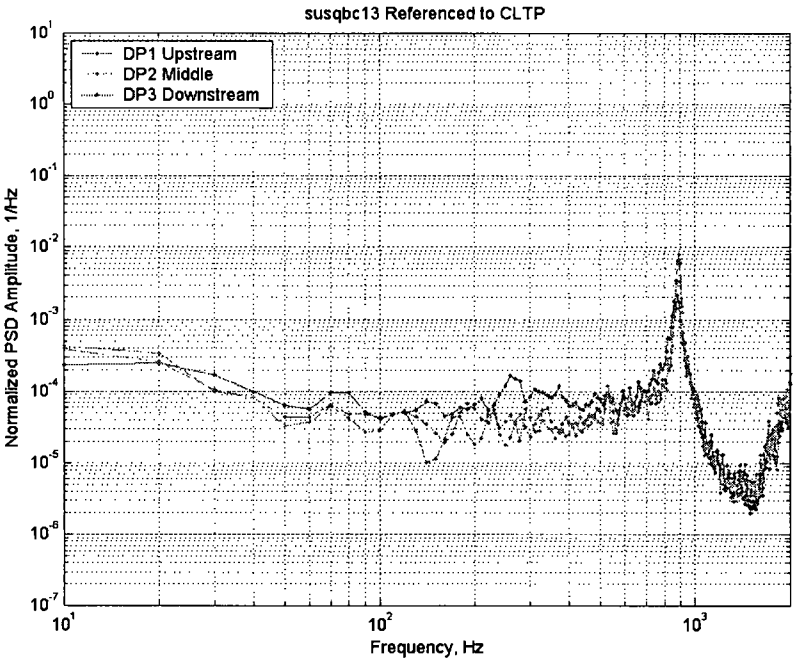

Figure A.13. Normalized PSD for B/C Test 13: Mach number = 0.1329.

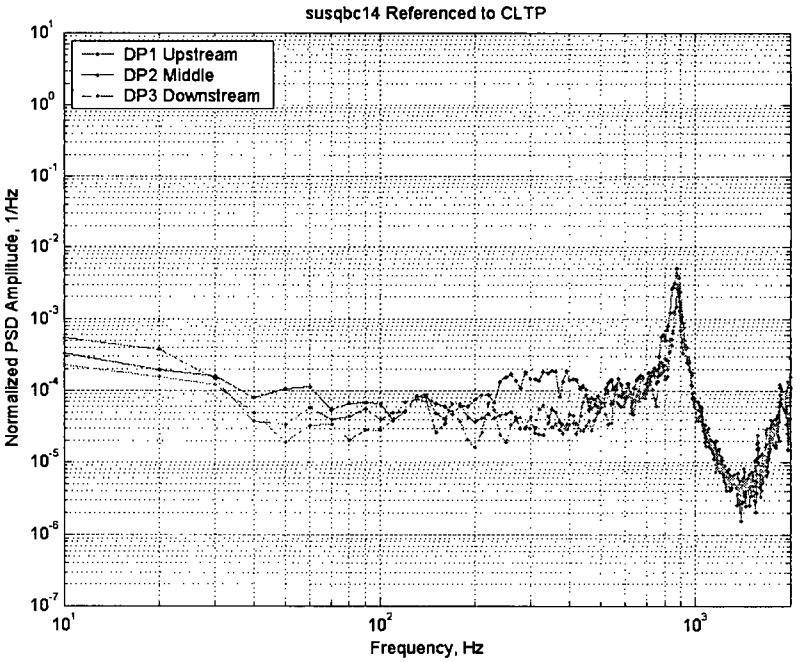

Figure A.14. Normalized PSD for B/C Test 14: Mach number = 0.1462.

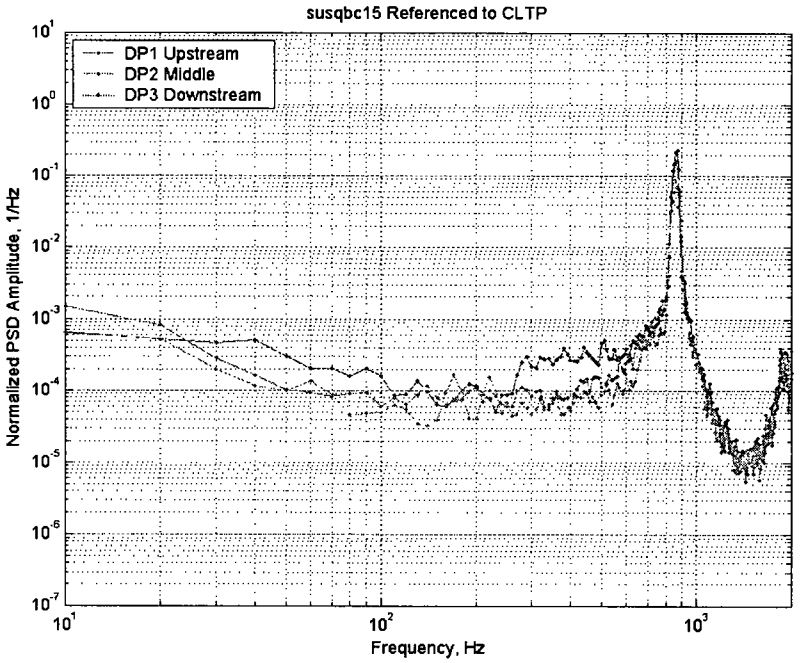

Figure A.15. Normalized PSD for B/C Test 15: Mach number = 0.1772.

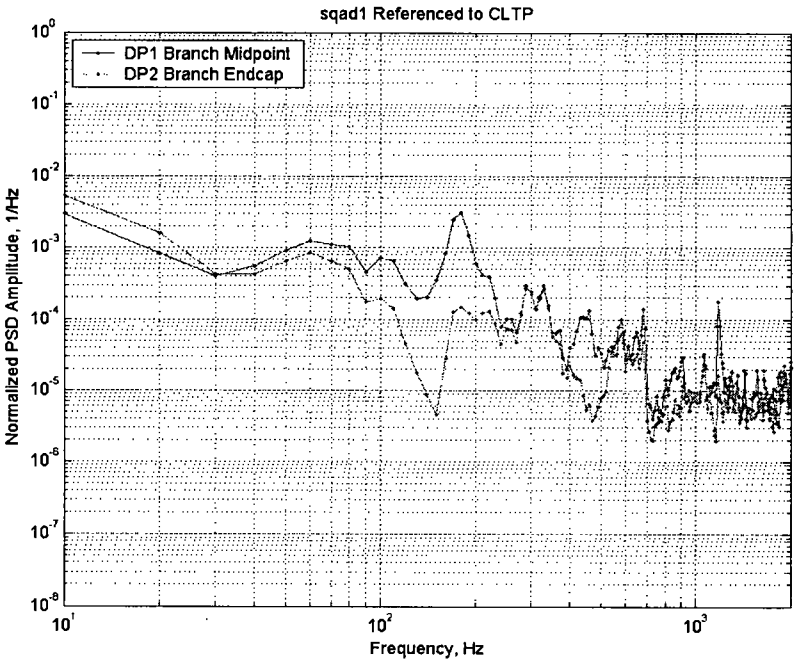

Figure A.16. Normalized PSD for A/D Test 1: Mach number = 0.2194.

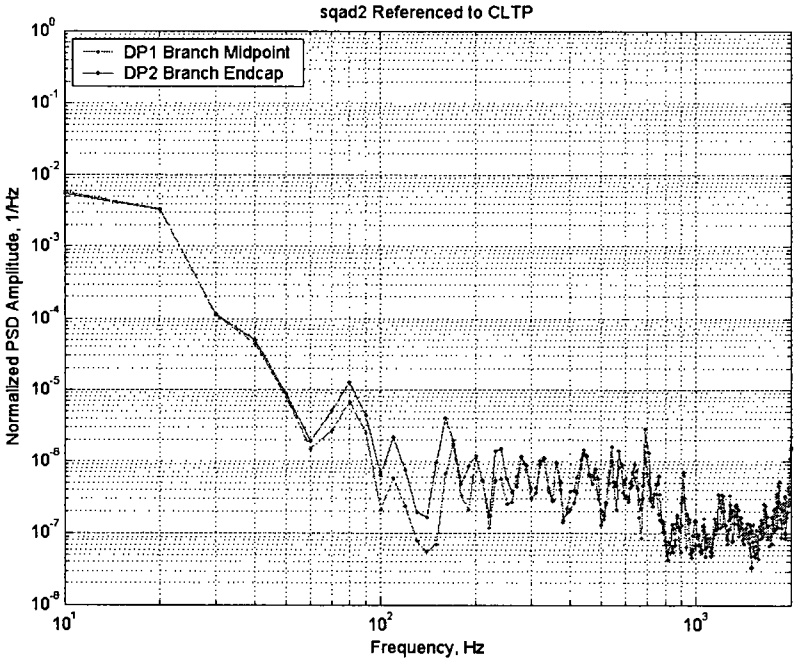

Figure A.17. Normalized PSD for A/D Test 2: Mach number = 0.0302.

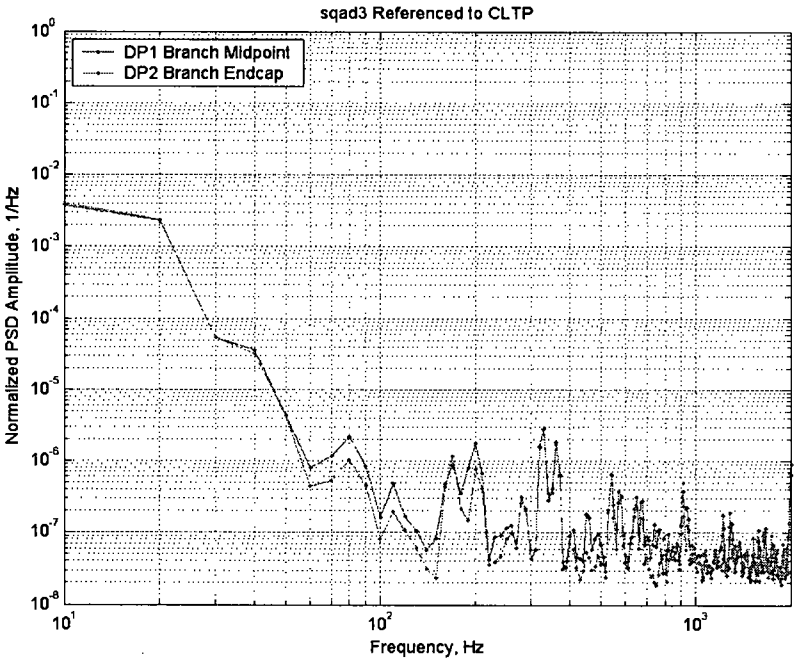

Figure A.18. Normalized PSD for A/D Test 3: Mach number = 0.0302.

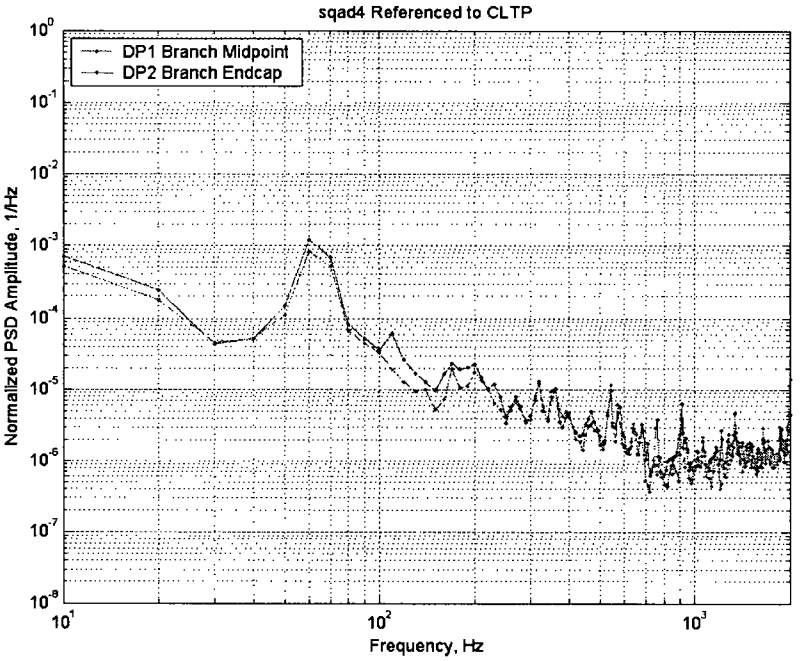

Figure A.19. Normalized PSD for A/D Test 4: Mach number = 0.1044.

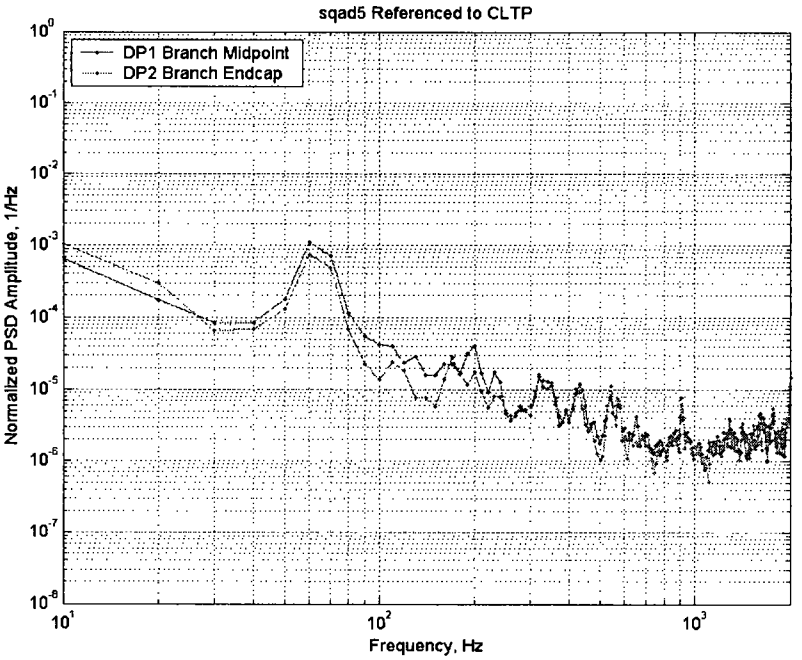

Figure A.20. Normalized PSD for A/D Test 5: Mach number = 0.1044.

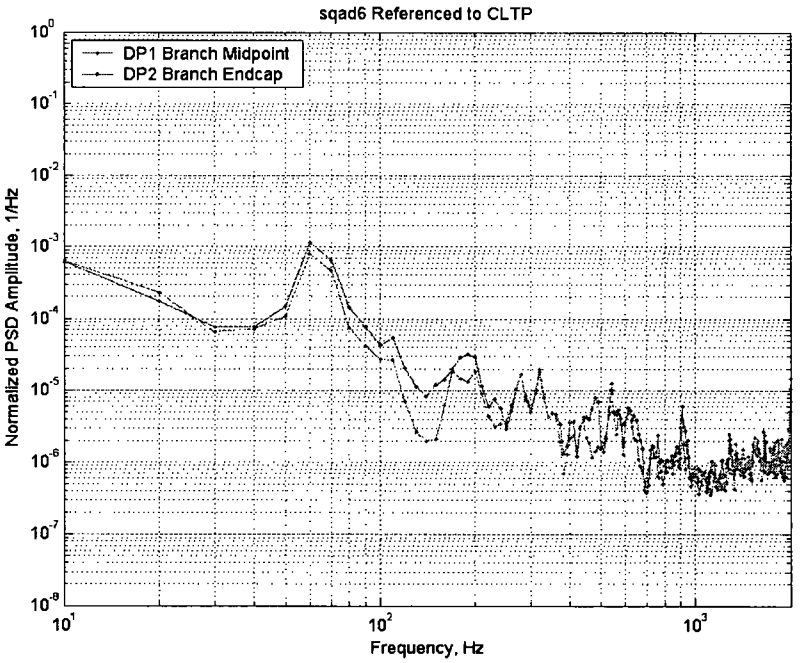

Figure A.21. Normalized PSD for A/D Test 6: Mach number = 0.1044.

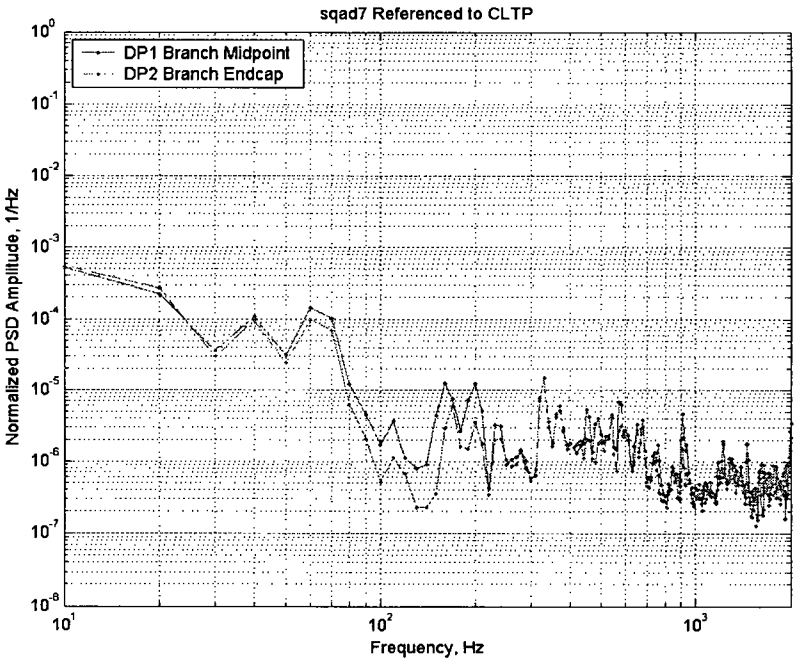

Figure A.22. Normalized PSD for A/D Test 7: Mach number = 0.0690.

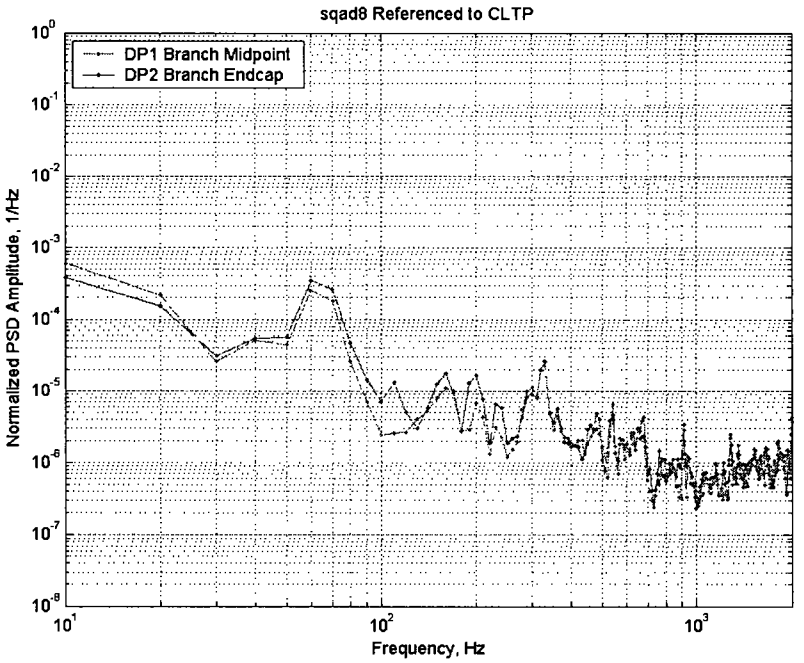

Figure A.23. Normalized PSD for A/D Test 8: Mach number = 0.0805.

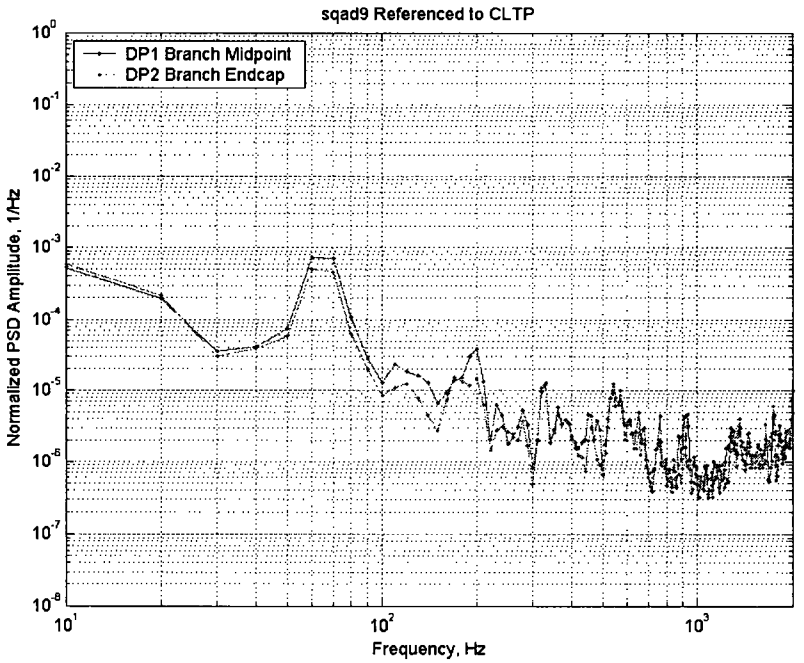

Figure A.24. Normalized PSD for A/D Test 9: Mach number = 0.0996.

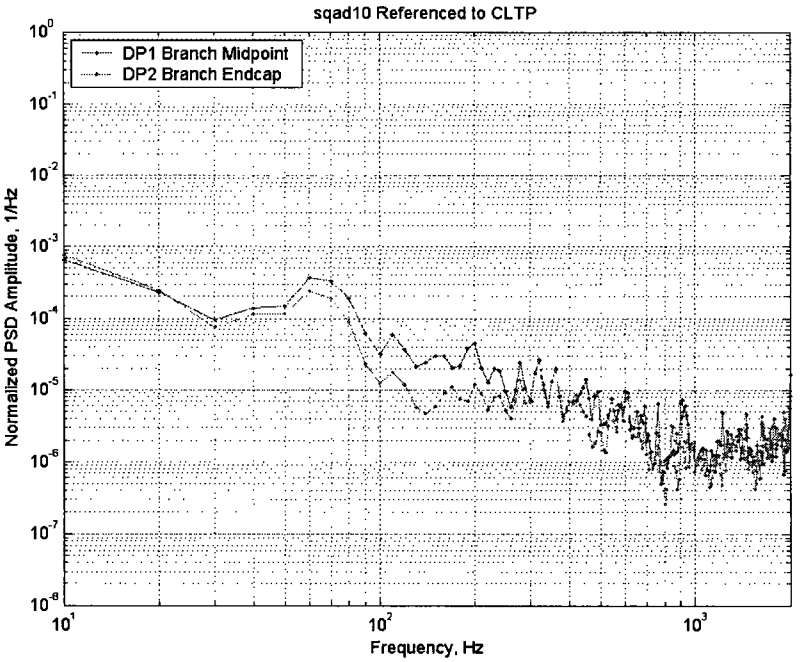

Figure A.25. Normalized PSD for A/D Test 10: Mach number = 0.1218.

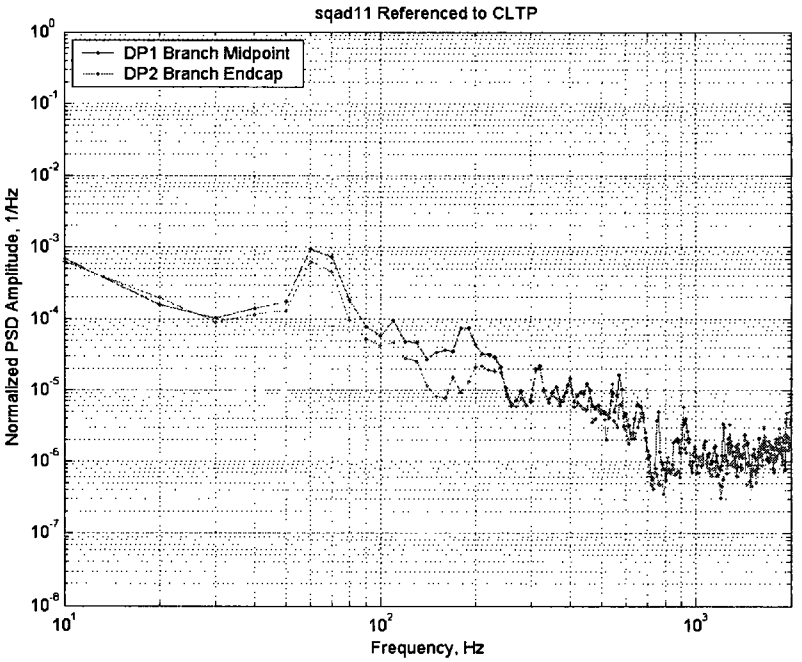

Figure A.26. Normalized PSD for A/D Test 11: Mach number = 0.1329.

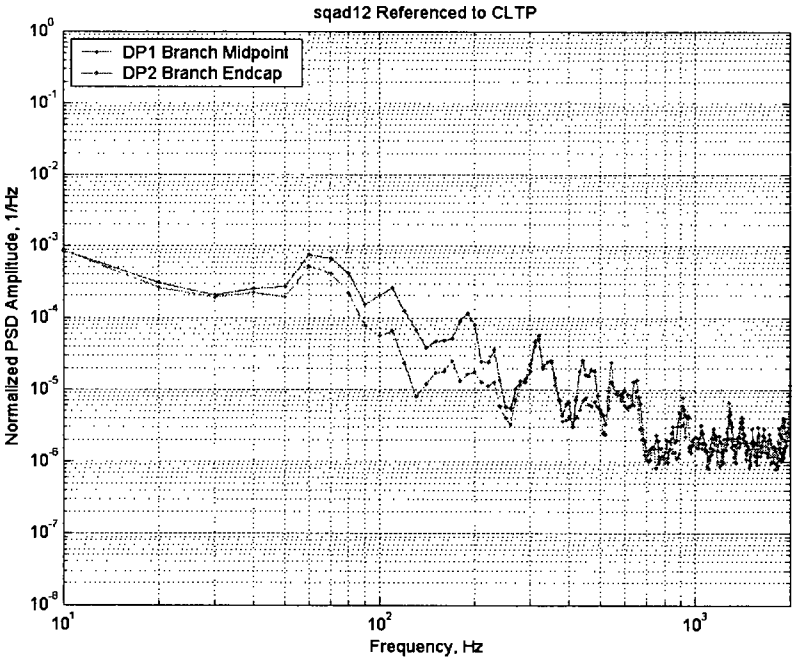

Figure A.27. Normalized PSD for A/D Test 12: Mach number = 0.1462.

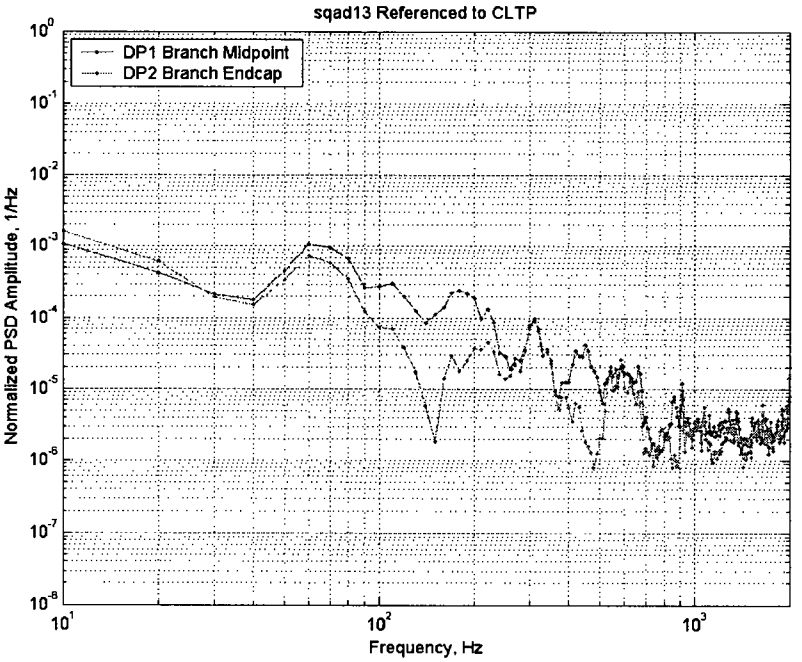

Figure A.28. Normalized PSD for A/D Test 13: Mach number = 0.1772.

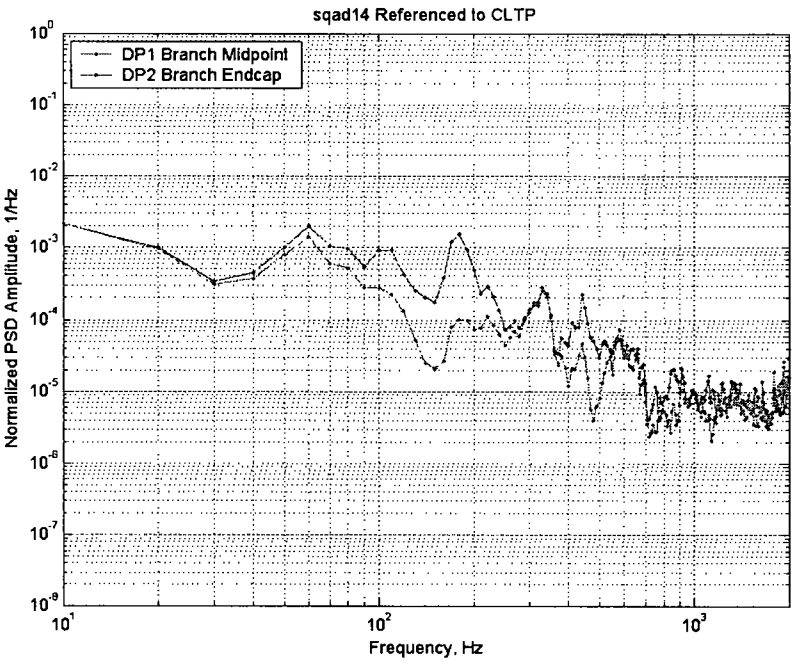

Figure A.29. Normalized PSD for A/D Test 14: Mach number = 0.2194.

Attachment 2 to PLA-6242
Appendix 3

Design And Fabrication Improvements For the Susquehanna Replacement Steam Dryers (Table & Figures For RAI 6(a))

GEH NON-PROPRIETARY INFORMATION

FOLLOW-UP REQUEST FOR ADDITIONAL INFORMATION
PROPOSED EXTENDED POWER UPRATE AMENDMENT
FOR SUSQUEHANNA UNITS 1 AND 2

GEH NON-PROPRIETARY INFORMATION

FOLLOW-UP REQUEST FOR ADDITIONAL INFORMATION
PROPOSED EXTENDED POWER UPRATE AMENDMENT
FOR SUSQUEHANNA UNITS 1 AND 2

Table 1

[[

GEH NON-PROPRIETARY INFORMATION

FOLLOW-UP REQUEST FOR ADDITIONAL INFORMATION
PROPOSED EXTENDED POWER UPRATE AMENDMENT
FOR SUSQUEHANNA UNITS 1 AND 2

]]

FOLLOW-UP REQUEST FOR ADDITIONAL INFORMATION
PROPOSED EXTENDED POWER UPRATE AMENDMENT
FOR SUSQUEHANNA UNITS 1 AND 2

[[

]]

Figure 1

GEH NON-PROPRIETARY INFORMATION

FOLLOW-UP REQUEST FOR ADDITIONAL INFORMATION
PROPOSED EXTENDED POWER UPRATE AMENDMENT
FOR SUSQUEHANNA UNITS 1 AND 2

[[

]]

Figure 2

[[

]]

Figure 3

FOLLOW-UP REQUEST FOR ADDITIONAL INFORMATION
PROPOSED EXTENDED POWER UPRATE AMENDMENT
FOR SUSQUEHANNA UNITS 1 AND 2

[[

]]

Figure 4

FOLLOW-UP REQUEST FOR ADDITIONAL INFORMATION
PROPOSED EXTENDED POWER UPRATE AMENDMENT
FOR SUSQUEHANNA UNITS 1 AND 2

[[

]]

Figure 5

[[

GEH NON-PROPRIETARY INFORMATION

FOLLOW-UP REQUEST FOR ADDITIONAL INFORMATION
PROPOSED EXTENDED POWER UPRATE AMENDMENT
FOR SUSQUEHANNA UNITS 1 AND 2

Figure 6

FOLLOW-UP REQUEST FOR ADDITIONAL INFORMATION
PROPOSED EXTENDED POWER UPRATE AMENDMENT
FOR SUSQUEHANNA UNITS 1 AND 2

[[

]]

Figure 7

FOLLOW-UP REQUEST FOR ADDITIONAL INFORMATION
PROPOSED EXTENDED POWER UPRATE AMENDMENT
FOR SUSQUEHANNA UNITS 1 AND 2

[[

]]

Figure 8

GEH NON-PROPRIETARY INFORMATION

FOLLOW-UP REQUEST FOR ADDITIONAL INFORMATION
PROPOSED EXTENDED POWER UPRATE AMENDMENT
FOR SUSQUEHANNA UNITS 1 AND 2

[[

]]

Figure 9

FOLLOW-UP REQUEST FOR ADDITIONAL INFORMATION
PROPOSED EXTENDED POWER UPRATE AMENDMENT
FOR SUSQUEHANNA UNITS 1 AND 2

[[

]]

Figure 10

FOLLOW-UP REQUEST FOR ADDITIONAL INFORMATION
PROPOSED EXTENDED POWER UPRATE AMENDMENT
FOR SUSQUEHANNA UNITS 1 AND 2

[[

]]

Figure 11

FOLLOW-UP REQUEST FOR ADDITIONAL INFORMATION
PROPOSED EXTENDED POWER UPRATE AMENDMENT
FOR SUSQUEHANNA UNITS 1 AND 2

[[

]]

Figure 12